Electronic Supplementary Material (ESI) for Journal of Materials Chemistry A.


**Thienochrysenocarbazole based organic dyes for transparent solar cells with over 10% efficiency**

Xinrui Xie, Danyang Sun, Yuefang Wei, Yi Yuan, Jing Zhang, Yutong Ren and Peng Wang*

*Department of Chemistry, Zhejiang University, Hangzhou 310028, China.*

**E-mail: pw2015@zju.edu.cn*

**Materials**. Tris(dibenzylideneacetone)dipalladium ($Pd_2(dba)_3$), palladium(II) acetate ($Pd(OAc)_2$), bis(triphenylphosphine)palladium(II) chloride ($Pd(PPh_3)_2Cl_2$), tris(1,1-dimethylethyl)phosphine (P(*t*-Bu)$_3$), methyl thiophene-3-carboxylate, tricyclohexylphosphinetetrafluroborate ($PCy_3{\cdot}HBF_4$), trimethylacetic acid (PivOH), Amberlyst 15, *n*-butyllithium (*n*-BuLi), chlorotrimethylstannane ($Me_3SnCl$), *N*-bromosuccinimide (NBS), potassium carbonate ($K_2CO_3$), cesium carbonate ($Cs_2CO_3$), potassium hydroxide (KOH), anhydrous toluene (PhMe), anhydrous tetrahydrofuran (THF), and phosphoric acid were purchased from Sigma-Aldrich. 3-Bromo-1-(2-hexyldecyl)-10-(4-((2-hexyldecyl)oxy)phenyl)-1*H*-phenanthro[1,10,9,8-*cdefg*]carbazole (**1**),[S1] (4-hexylphenyl)magnesium bromide,[S2] butyl 4-(benzo[*c*][1,2,5]thiadiazol-4-yl)benzoate,[S3] and butyl 4-((7-bromobenzo[*c*][1,2,5]thiadiazol-4-yl)ethynyl)benzoate[S4] were prepared according to the protocols described in the corresponding literatures. Other chemicals were purchased and used without further purification. The synthetic routes to C296 and C298 are illustrated in Scheme S1 and the preparation details are described as follows.

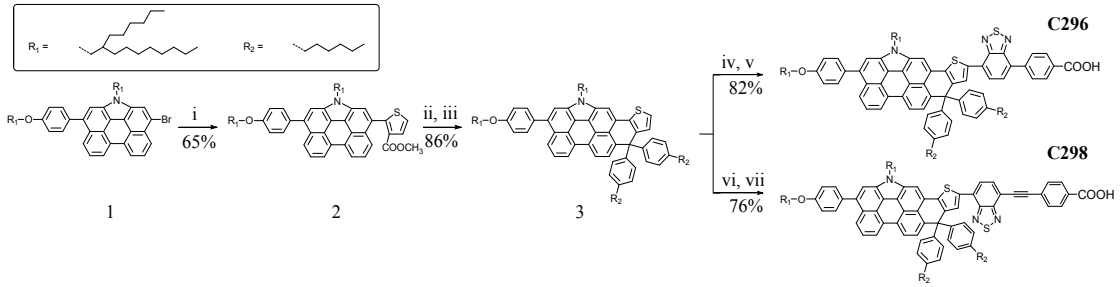


Scheme S1. Synthetic routes to C296 and C298. Reagents and conditions: (i) methyl thiophene-3-carboxylate, $Pd(OAc)_2$, $PCy_3{\cdot}HBF_4$, PivOH, $K_2CO_3$, toluene, reflux, 24 h; (ii) (4-hexylphenyl)magnesium bromide, THF, reflux, 6 h; (iii) Amberlyst 15, toluene, reflux, 6 h; (iv) *n*-BuLi, THF, −78 °C, 0.5 h; $Sn(CH_3)_3Cl$, R.T., overnight; then butyl 4-(7-bromobenzo[*c*][1,2,5]thiadiazol-4-yl)benzoate, $Pd(PPh_3)_2Cl_2$, toluene, reflux, 6 h; (v) KOH, THF/$H_2O$ (3/1, *v*/*v*), reflux, overnight; hydrochloric acid; (vi) *n*-BuLi, THF, −78 °C, 0.5 h; $Sn(CH_3)_3Cl$, R.T., overnight; then 4-((7-bromobenzo[*c*][1,2,5]thiadiazol-4-yl)ethynyl)benzoate, $Pd_2(dba)_3$, P(*t*-Bu)$_3$, CsF, dioxane, reflux, 6 h; (vii) KOH, THF/$H_2O$ (3/1, *v*/*v*), reflux, overnight; phosphoric acid.

*2-(1-(2-Hexyldecyl)-10-(4-((2-hexyldecyl)oxy)phenyl)-1H-phenanthro[1,10,9,8-cdefg]carbazol-3-yl)thiophene-3-carboxylate (**2**)*

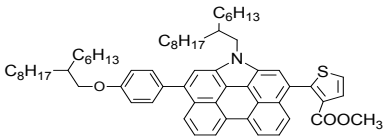

In a dried Schlenk tube were dissolved **1** (1.77 g, 2.00 mmol), methyl thiophene-3-carboxylate (0.34 g, 2.40 mmol), $K_2CO_3$ (0.41 g, 3.00 mmol), $Pd(OAc)_2$ (33 mg, 0.12 mmol), $PCy_3.HBF_4$ (88 mg, 0.24 mmol), and PivOH (61 mg, 0.60 mmol) in toluene (20 mL) in a nitrogen-filled glovebox. The reaction mixture was stirred under reflux for 24 h. The mixture was extracted three times with chloroform before the organic phase was washed with water and dried over anhydrous sodium sulfate. After solvent removal under reduced pressure, the crude product was purified by column chromatography (toluene/petroleum ether 60–90 °C, 1/5, *v*/*v*) on silica gel to yield a yellow oil as the desired product **2** (1.23 g, 65% yield). $^1$H NMR (400 MHz, $CDCl_3$) $\delta$: 8.68 (s, 1H), 8.15 (s, 1H), 7.79–7.75 (m, 2H), 7.74–7.70 (m, 2H), 7.64 (d, $J$ = 8.2 Hz, 2H), 7.41 (d, $J$ = 5.4 Hz, 1H), 7.12 (d, $J$ = 8.6 Hz, 2H), 4.55 (d, $J$ = 7.3 Hz, 2H), 3.97 (d, $J$ = 5.6 Hz, 2H), 3.40 (s, 3H), 2.31–2.29 (m, 1H), 1.89–1.85 (m, 1H), 1.58–1.51 (m, 2H), 1.48–1.46 (m, 2H), 1.42–1.26 (m, 32H), 1.19–1.17 (m, 12H), 0.94–0.89 (m, 6H), 0.84–0.78 (m, 6H). $^{13}$C NMR (100 MHz, $CDCl_3$) $\delta$: 164.16, 159.07, 150.30, 134.26, 131.48, 130.72, 129.74, 124.73, 124.46, 121.00, 116.73, 114.69, 71.29, 51.59, 50.28, 40.08, 38.31, 32.16, 30.16, 29.86, 29.47, 26.59, 22.93, 22.92, 22.82, 14.35, 14.29, 14.25. HR-MS (MALDI-TOF) *m*/*z* Calcd. for ($C_{64}H_{83}NO_3S$): 945.60937. Found: 946.60712 ([$M^+$]). Anal. Calcd. for $C_{64}H_{83}NO_3S$: C, 81.22%; H, 8.84%; N, 1.48%. Found: C, 81.23%; H, 8.85%; N, 1.45%.

*11-(2-Hexyldecyl)-13-(4-((2-hexyldecyl)oxy)phenyl)-6,6-bis(4-hexylphenyl)-6,11-dihydrothieno[3',2':8,9]chryseno[10,11,12,1-bcdefg]carbazole (**3**)*

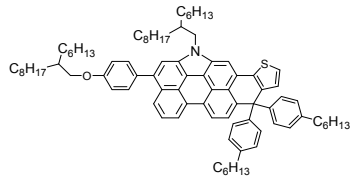

To a dried Schlenk tube with **2** (945 mg, 1.00 mmol) in THF (10 mL) was added (4-hexylphenyl)magnesium bromide (2.50 mL, 2 M in THF, 5.00 mmol) in one portion via syringe. The mixture was slowly warmed up and stirred under reflux for 6 h. Water was slowly added to terminate the reaction and the mixture was poured into cold 1 M hydrochloric acid aqueous solution. The mixture was extracted three times with chloroform before the organic phase was washed with water and dried

over anhydrous sodium sulfate. After solvent removal under reduced pressure, the residue tertiary alcohol was used in the next reaction directly. In a dried Schlenk tube were added the above tertiary alcohol and Amberlyst 15 (0.50 g) in 20 mL toluene, which was refluxed for 6 h. After filtering the solid catalyst, the filtrate was washed with water and dried over anhydrous sodium sulfate. After solvent removal under reduced pressure, the crude product was purified by column chromatography (toluene/petroleum ether 60–90 °C, 1/10, *v*/*v*) on silica gel to yield an orange oil as the desired product **3** (1.05 g, 86% yield). $^{1}$H NMR (400 MHz, THF-$d_8$) $\delta$: 8.60 (d, $J$ = 2.6 Hz, 1H), 8.58 (d, $J$ = 3.4 Hz, 1H), 8.07 (d, $J$ = 8.2 Hz, 1H), 8.01 (s, 1H), 7.75 (s, 1H), 7.70–7.63 (m, 2H), 7.59 (d, $J$ = 8.3 Hz, 2H), 7.22–7.20 (m, 5H), 7.09 (d, $J$ = 8.4 Hz, 2H), 7.05–7.03 (m, 4H), 6.89 (d, $J$ = 5.2 Hz, 1H), 4.65 (d, $J$ = 7.0 Hz, 2H), 3.98 (d, $J$ = 5.3 Hz, 2H), 2.56–2.52 (m, 4H), 2.37 (br, 1H), 1.87 (br, 1H), 1.59–1.54 (m, 6H), 1.50–1.43 (m, 12H), 1.36–1.30 (m, 33H), 1.23–1.19 (m, 17H), 0.93–0.91 (m, 6H), 0.89–0.85 (m, 6H), 0.80–0.78 (m, 6H). $^{13}$C NMR (100 MHz, THF-$d_8$) $\delta$: 160.02, 147.32, 145.04, 142.22, 141.57, 138.44, 137.77, 135.31, 133.83, 133.53, 132.16, 131.64, 131.48, 130.71, 129.41, 129.35, 128.74, 127.92, 126.91, 125.86, 125.46, 125.08, 124.92, 123.98, 123.17, 122.81, 121.55, 118.35, 118.09, 115.35, 115.09, 106.97, 71.70, 59.23, 50.58, 40.94, 39.36, 36.51, 33.07, 33.05, 32.99, 32.96, 32.86, 32.75, 32.64, 31.24, 31.10, 30.91, 30.78, 30.69, 30.51, 30.42, 30.28, 28.05, 28.03, 27.51, 27.48, 23.78, 23.75, 23.69, 23.67, 23.64, 14.66, 14.65, 14.63, 14.61, 14.59. HR-MS (MALDI-TOF) *m*/*z* Calcd. for ($C_{87}H_{113}NOS$): 1219.85429. Found: 1220.85173 ([$M^+$]). Anal. Calcd. for $C_{87}H_{113}NOS$: C, 85.59%; H, 9.33%; N, 1.15%. Found: C, 85.61%, H, 9.39%; N, 1.16%.

*4-(7-(11-(2-Hexyldecyl)-13-(4-((2-hexyldecyl)oxy)phenyl)-6,6-bis(4-hexylphenyl)-6,11-dihydrothieno[3',2':8,9]chryseno[10,11,12,1-bcdefg]carbazol-8-yl)benzo[c][1,2,5]thiadiazol-4-yl)benzoic acid (**C296**)*

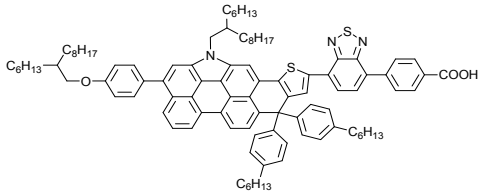


In a flame-dried three-neck round-bottom flask was dissolved **3** (610 mg, 0.50 mmol) in THF (10 mL) and cooled to −78 °C using a dry ice/acetone cold bath. Under argon, *n*-BuLi (0.38 mL, 1.6 M in hexanes, 0.60 mmol) was added dropwise, and the reaction mixture was stirred for 0.5 h at −78 °C.

After trimethylstannyl chloride (119 mg, 0.60 mmol) was added in one portion via syringe, the mixture was slowly warmed up and stirred at room temperature for 2 h. Water was slowly added to terminate the reaction and the mixture was extracted three times with diethyl ether before the organic phase was washed with water and dried over anhydrous sodium sulfate. After solvent removal under reduced pressure, the crude product 11-(2-hexyldecyl)-13-(4-((2-hexyldecyl)oxy)phenyl)-6,6-bis(4-hexylphenyl)-8-(trimethylstannyl)-6,11-dihydrothieno[3',2':8,9]chryseno[10,11,12,1-*bcdefg*]carbazole was used to the further reaction without purification. In a dried Schlenk tube were dissolved 11-(2-hexyldecyl)-13-(4-((2-hexyldecyl)oxy)phenyl)-6,6-bis(4-hexylphenyl)-8-(trimethylstannyl)-6,11-dihydrothieno[3',2':8,9]chryseno[10,11,12,1-*bcdefg*]carbazole and butyl 4-(7-bromobenzo[*c*][1,2,5]thiadiazol-4-yl)benzoate (294 mg, 0.75 mmol), and $Pd(PPh_3)_2Cl_2$ (22 mg, 0.03 mmol) in toluene (10 mL). The reaction mixture was stirred under reflux for 6 h. Water was added and the mixture was extracted three times with chloroform before the organic phase was washed with water and dried over anhydrous sodium sulfate. After solvent removal under reduced pressure, the crude product was purified by column chromatography (toluene/petroleum ether 60–90 °C, 2/1, *v*/*v*) on silica gel to yield a black powder as the desired butyl ester. In a three-neck round-bottom flask were dissolved butyl ester (643 mg, 0.42 mmol) and KOH (235 mg, 4.20 mmol) in a solvent mixture of THF/$H_2O$ (8 mL, 3/1, *v*/*v*). The reaction mixture was refluxed overnight and then cooled to room temperature. Chloroform was added before the organic phase was washed with 0.1 M hydrochloric acid and deionized water in turn and then dried over anhydrous sodium sulfate. After solvent removal under reduced pressure, the crude product was purified by column chromatography (chloroform/methanol, 10/1, *v*/*v*) on silica gel to yield a black solid as the desired product **C296** (612 mg, 82% yield). M. p. 122–123 °C. $^1$H NMR (400 MHz, THF-$d_8$) $\delta$: 8.65 (d, $J$ = 8.0 Hz, 1H), 8.64 (d, $J$ = 7.2 Hz, 1H), 8.13–8.12 (m, 3H), 8.09 (d, $J$ = 8.2 Hz, 1H), 7.99 (d, $J$ = 8.2 Hz, 2H), 7.79 (d, $J$ = 6.6 Hz, 2H), 7.73–7.69 (m, 1H), 7.55–7.51 (m, 5H), 7.47 (d, $J$ = 7.5 Hz, 1H), 7.41 (d, $J$ = 8.2 Hz, 2H), 7.33 (s, 1H), 7.22 (d, $J$ = 8.2 Hz, 4H), 7.04 (d, $J$ = 8.3 Hz, 2H), 3.98 (d, $J$ = 5.0 Hz, 2H), 3.86 (br, 2H), 2.61 (t, $J$ = 7.4 Hz, 4H), 2.05–2.03 (m, 1H), 1.88–1.87 (m, 1H), 1.64–1.60 (m, 6H), 1.52–1.47 (m, 6H), 1.38–1.26 (m, 30H), 1.14 (br, 20H), 0.95–0.91 (m, 6H), 0.85–0.83 (m, 6H), 0.79–0.75 (m, 6H). $^{13}$C NMR (100 MHz, THF-$d_8$) $\delta$: 175.83, 167.70, 159.92, 154.21, 153.24, 147.74, 145.75, 142.07, 142.03, 141.84, 140.22, 138.44, 137.12, 135.07, 133.70, 133.38, 132.34, 132.21, 131.34, 131.16, 131.02, 130.68, 130.63, 129.90, 129.49, 129.23, 129.04, 128.11, 127.51, 126.18, 125.74, 125.37, 124.70, 123.97,

122.84, 121.60, 118.43, 117.74, 115.28, 114.77, 107.51, 71.73, 59.21, 50.22, 40.42, 39.37, 36.60, 36.40, 33.09, 33.07, 33.02, 32.99, 32.90, 32.84, 32.66, 32.59, 31.27, 31.06, 30.93, 30.89, 30.87, 30.80, 30.72, 30.64, 30.53, 30.45, 30.33, 28.19, 28.08, 28.05, 27.32, 27.29, 26.59, 23.80, 23.77, 23.70, 23.64, 14.72, 14.70, 14.65, 14.63, 14.60. HR-MS (MALDI-TOF) *m*/*z* Calcd. for ($C_{100}H_{119}N_3O_3S_2$): 1473.86929. Found: 1473.86526 ([$M^+$]). Anal. Calcd. for $C_{100}H_{119}N_3O_3S_2$: C, 81.42%; H, 8.13%; N, 2.85%; Found: C, 81.46%; H, 8.16%; N, 2.81%.

*4-(7-((11-(2-Hexyldecyl)-13-(4-((2-hexyldecyl)oxy)phenyl)-6,6-bis(4-hexylphenyl)-6,11-dihydrothieno[3',2':8,9]chryseno[10,11,12,1-bcdefg]carbazol-8-yl)ethynyl)benzo[c][1,2,5]thiadiazol-4-yl)benzoic acid (**C298**)*

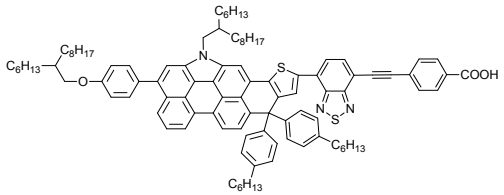


11-(2-Hexyldecyl)-13-(4-((2-hexyldecyl)oxy)phenyl)-6,6-bis(4-hexylphenyl)-8-(trimethylstannyl)-6,11-dihydrothieno[3',2':8,9]chryseno[10,11,12,1-*bcdefg*]carbazole prepared as above from **3** (610 mg, 0.50 mmol), butyl 4-((7-bromobenzo[*c*][1,2,5]thiadiazol-4-yl)ethynyl)benzoate (311 mg, 0.75 mmol), and $Pd(PPh_3)_2Cl_2$ (22 mg, 0.03 mmol) were dissolved in toluene (10 mL) in a dried round bottom. The reaction mixture was refluxed under argon for 6 h and cooled to room temperature. The mixture was extracted three times with chloroform. The organic phase was combined, washed with water, and dried over anhydrous sodium sulfate. After solvent removal under reduced pressure, the residue was purified by column chromatography (toluene/petroleum ether 60–90 °C, 2/1, *v*/*v*) on silica gel to yield a black powder as the desired butyl ester. In a two-neck round bottom were dissolved the butyl ester (591 mg, 0.38 mmol) and KOH (225 mg, 4.10 mmol) in a mixed solvent of THF/$H_2O$ (8 mL, 3/1, *v*/*v*). The reaction mixture was refluxed overnight and then cooled to room temperature. Chloroform was added to extract the mixture. The organic phase was combined, and washed with 0.1 M phosphoric acid and deionized water in turn. After the organic phase was dried over anhydrous sodium sulfate, the solvent was removed under reduced pressure. The residue was purified by column chromatography (chloroform/methanol, 10/1, *v*/*v*) on silica gel to yield a black solid as the desired product **C298** (570 mg, 76% yield). M. p. 154–156 °C. $^1$H NMR (400 MHz, THF-$d_8$) $\delta$: 8.65 (d, $J$ = 7.9 Hz, 2H),

8.12–8.04 (m, 4H), 7.77–7.65 (m, 6H), 7.62 (s, 1H), 7.54–7.38 (m, 7H), 7.17–7.13 (m, 4H), 7.08 (d, *J* = 8.5 Hz, 2H), 8.09 (d, *J* = 8.2 Hz, 1H), 8.00 (d, *J* = 8.2 Hz, 2H), 7.80 (d, *J* = 6.6 Hz, 2H), 7.74–7.70 (m, 1H), 4.44-4.43 (m, 2H), 4.00–3.99 (m, 2H), 2.59–2.56 (m, 4H), 2.31-2.28 (m, 1H), 1.88–1.85 (m, 1H), 1.64–1.56 (m, 6H), 1.51–1.43 (m, 6H), 1.37–1.27 (m, 38H), 1.22–1.16 (m, 14H), 0.94–0.90 (m, 6H), 0.87–0.83 (m, 6H), 0.78–0.75 (m, 6H). $^{13}$C NMR (100 MHz, THF-$d_8$) $\delta$: 167.16, 160.04, 156.15, 152.59, 147.46, 146.11, 141.86, 141.82, 140.95, 138.84, 136.64, 135.16, 134.08, 133.99, 133.55, 132.79, 132.49, 132.19, 131.95, 131.38, 130.93, 130.87, 130.75, 129.53, 129.34, 128.96, 128.84, 128.41, 126.14, 125.81, 125.53, 125.34, 125.02, 124.78, 123.96, 122.88, 121.72, 118.84, 117.94, 115.33, 115.04, 107.70, 96.20, 89.59, 71.72, 59.11, 40.75 39.37, 36.55, 33.08, 33.07, 33.00, 32.97, 32.85, 32.65, 31.25, 31.11, 30.92, 30.80, 30.69, 30.52, 30.45, 30.31, 28.06, 28.04, 27.42, 23.78, 23.76, 23.71, 23.65, 14.65, 14.64, 14.59, 14.57. HR-MS (MALDI-TOF) *m*/*z* Calcd. for ($C_{102}H_{119}N_3O_3S_2$): 1497.86929. Found: 1497.86555 ([$M^+$]). Anal. Calcd. for $C_{102}H_{119}N_3O_3S_2$: C, 81.72%; H, 8.00%; N, 2.80%; Found: C, 81.77%; H, 8.04%; N, 2.71%.

## Notes and references


[S1] Z. Yao, H. Wu, Y. Ren, Y. Guo and P. Wang, *Energy Environ. Sci.*, 2015, **8**, 1438.

[S2] N. Cai, R. Li, Y. Wang, M. Zhang and P. Wang, *Energy Environ. Sci*., 2013, **6**, 139.

[S3] L. Yang, Y. Ren, Z. Yao, C. Yan, W. Ma, and P. Wang, *J. Phys. Chem. C*, 2015, **119**, 980.

[S4] Z. Yao, H. Wu, Y. Li, J. Wang, J. Zhang, M. Zhang, Y. Guo and P. Wang, *Energy Environ. Sci.*, 2015, **8**, 3192.

**Table S1** Theoretical and experimental absorption maxima, transition assignments, energy levels, and energy gaps

| Dye | Solvent | $E_{H}^{B3LYP}$ [eV] | $E_{H}^{CV}$ [eV] | $E_{L}^{B3LYP}$ [eV] | $E_{L}^{CV}$ [eV] | $\Delta E_{L/H}^{B3LYP}$ [eV] | $E_{L/H}^{CV}$ [eV] | $\Delta E_{L+1/H}^{B3LYP}$ [eV] | $\Delta E_{L/H-1}^{B3LYP}$ [eV] | $\lambda_{ABS,MAX}^{TD\text{-}MPW1K}$ [nm] | Transition |
|---|---|---|---|---|---|---|---|---|---|---|---|
| C296 | PhMe | –4.89 | / | –2.89 | / | 2.00 | / | 2.77 | 2.97 | 568 | H→L (88.7%); H→L+1 (4.8%); H–1→L (6.5%) |
| C298 | PhMe | –4.91 | / | –3.03 | / | 1.88 | / | 2.76 | 2.78 | 603 | H→L (89.5%); H→L+1 (3.3%); H–1→L (7.2%) |
| C296 | THF | –4.96 | –4.97 | –2.93 | –3.22 | 2.03 | 1.75 | 2.77 | 3.00 | 517 | H→L (74.4%); H→L+1 (13.8%); H–1→L (11.8%) |
| C298 | THF | –4.97 | –4.98 | –3.08 | –3.44 | 1.89 | 1.54 | 2.76 | 2.79 | 595 | H→L (89.6%); H→L+1 (3.3%); H–1→L (7.2%) |

H and L stand for HOMO and LUMO. Theoretical energy levels and energy gaps ( $E_{H}^{B3LYP}$, $E_{L}^{B3LYP}$, $\Delta E_{L/H}^{B3LYP}$, $\Delta E_{L+1/H}^{B3LYP}$, and $\Delta E_{L/H-1}^{B3LYP}$ ) were obtained from DFT calculation of dye molecules in PhMe or THF at the B3LYP/6-311G(d,p) level. Theoretical absorption maxima ( $\lambda_{ABS,MAX}^{TD\text{-}MPW1K}$ ) were obtained from TD-DFT calculations at the TD-MPW1K/6-311G(d,p) level for dye molecules in PhMe or THF. The experimental HOMO and LUMO energy levels ( $E_{H}^{CV}$ and $E_{L}^{CV}$ ) vs vacuum and LUMO/HOMO energy gaps ( $\Delta E_{L/H}^{CV}$ ) were estimated from cyclic voltammograms presented in Fig. 2a.

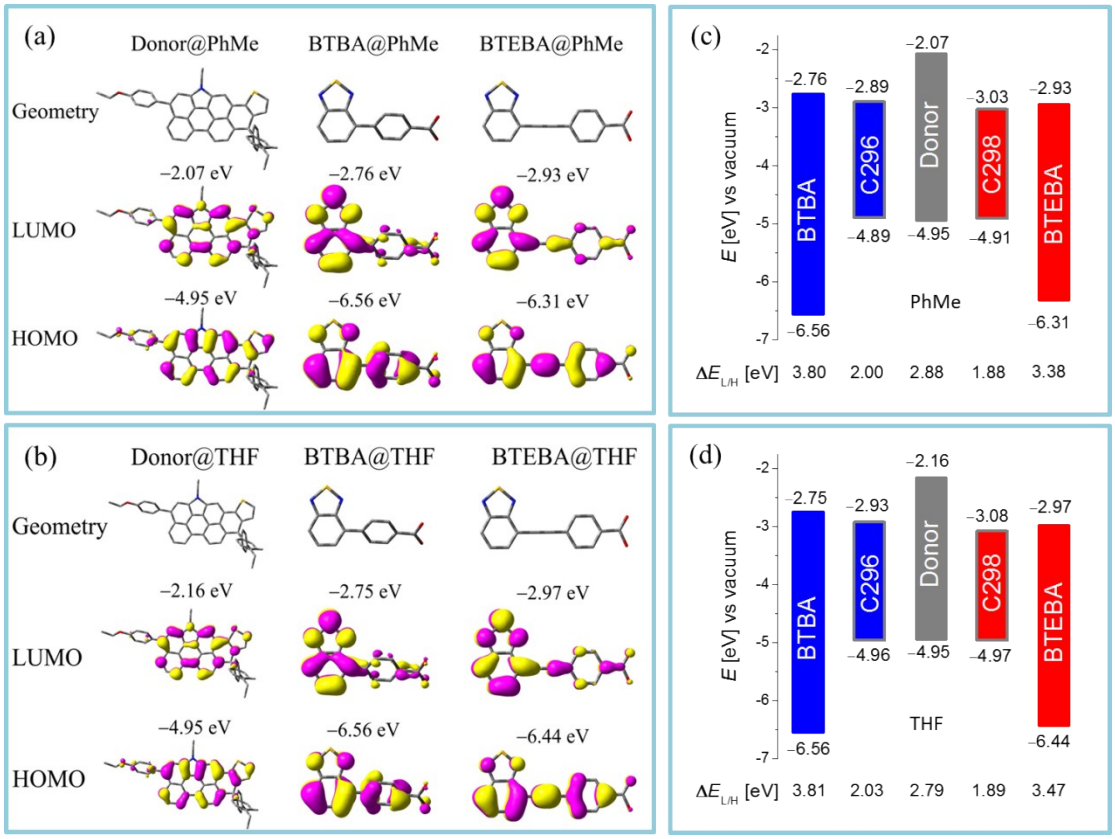


**Fig. S1** (a,b) Optimized molecular geometries and contour plots of HOMOs and LUMOs of electron-donor (compound 3), BTBA, and BTEBA in PhMe (a) and THF (b). The large aliphatic chains were replaced with ethyl to improve the computational efficiency. The isodensity value is fixed at 0.03. LUMO and HOMO energy levels are also given in panels a and b. (c,d) Theoretical LUMO energy levels (values above color bars), HOMO energy levels (values under color bars), and LUMO/HOMO energy gaps ( $\Delta E_{L/H}$ ) of dye molecules in PhMe (c) and THF (d) as well as their electron-donor (compound 3) and electron-accpetors (BTBA and BTEBA).

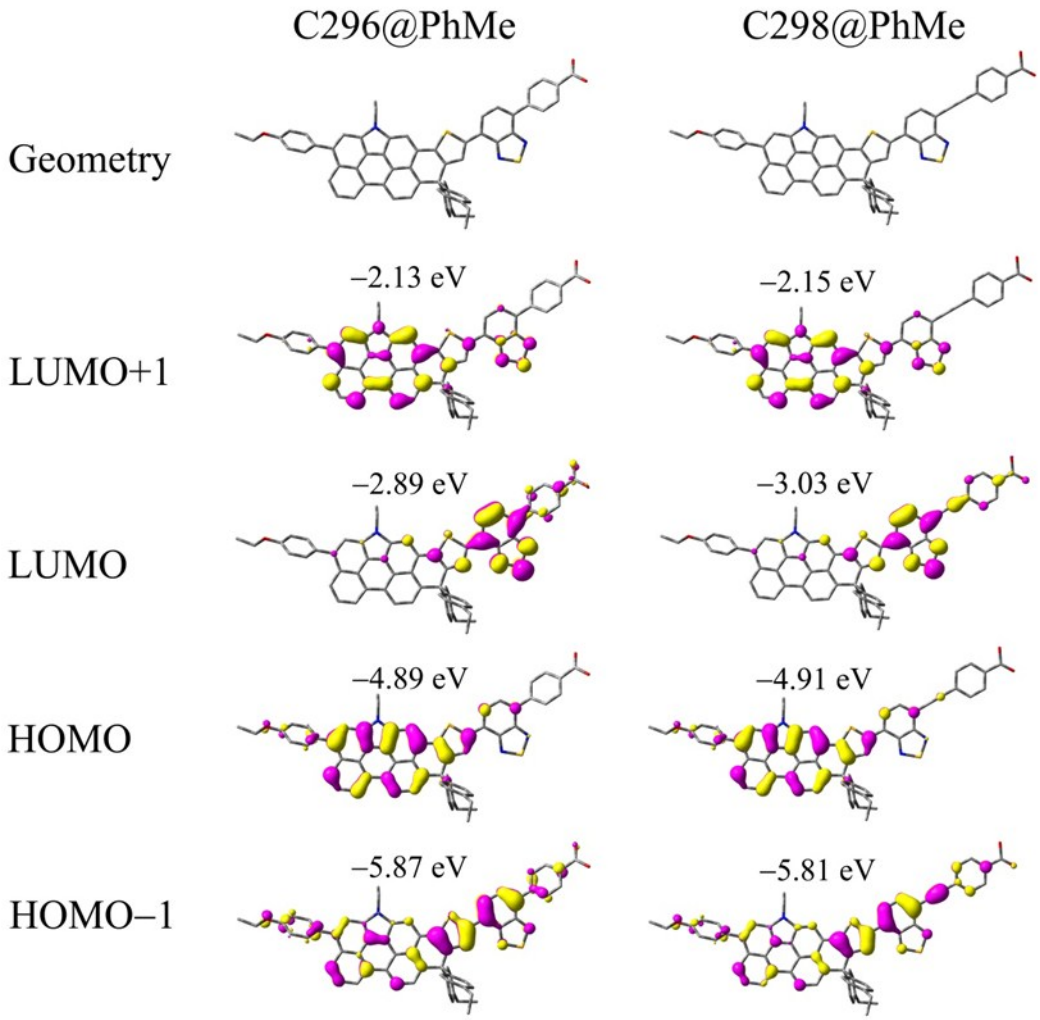


**Fig. S2** Optimized molecular geometries and contour plots of the $S_1^{vert} \leftarrow S_0$ transition related molecular orbitals of C296 and C298 in PhMe. The large aliphatic chains were replaced with ethyl to improve the computational efficiency. The isodensity value is fixed at 0.03.

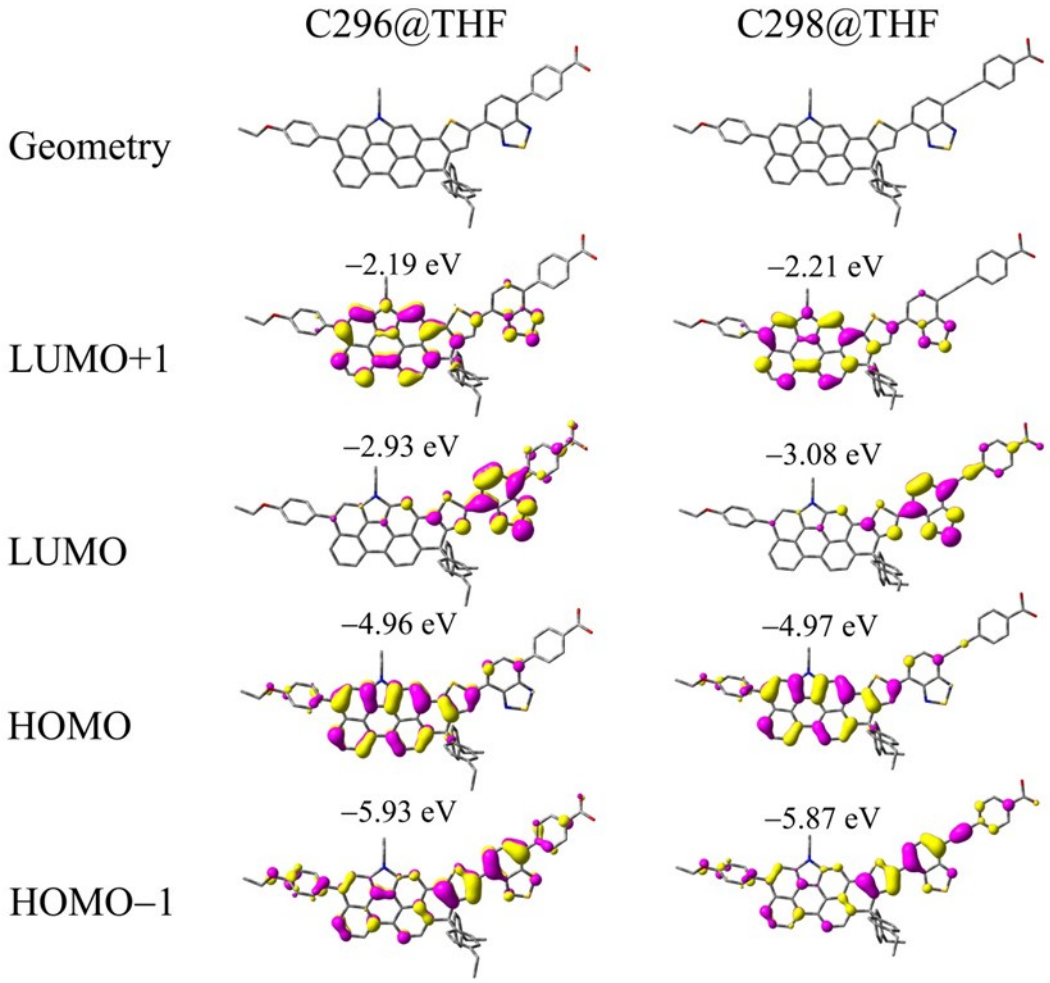


**Fig. S3** Optimized molecular geometries and contour plots of the $S_1^{vert} \leftarrow S_0$ transition related molecular orbitals of C296 and C298 in THF. The large aliphatic chains were replaced with ethyl to improve the computational efficiency. The isodensity value is fixed at 0.03.

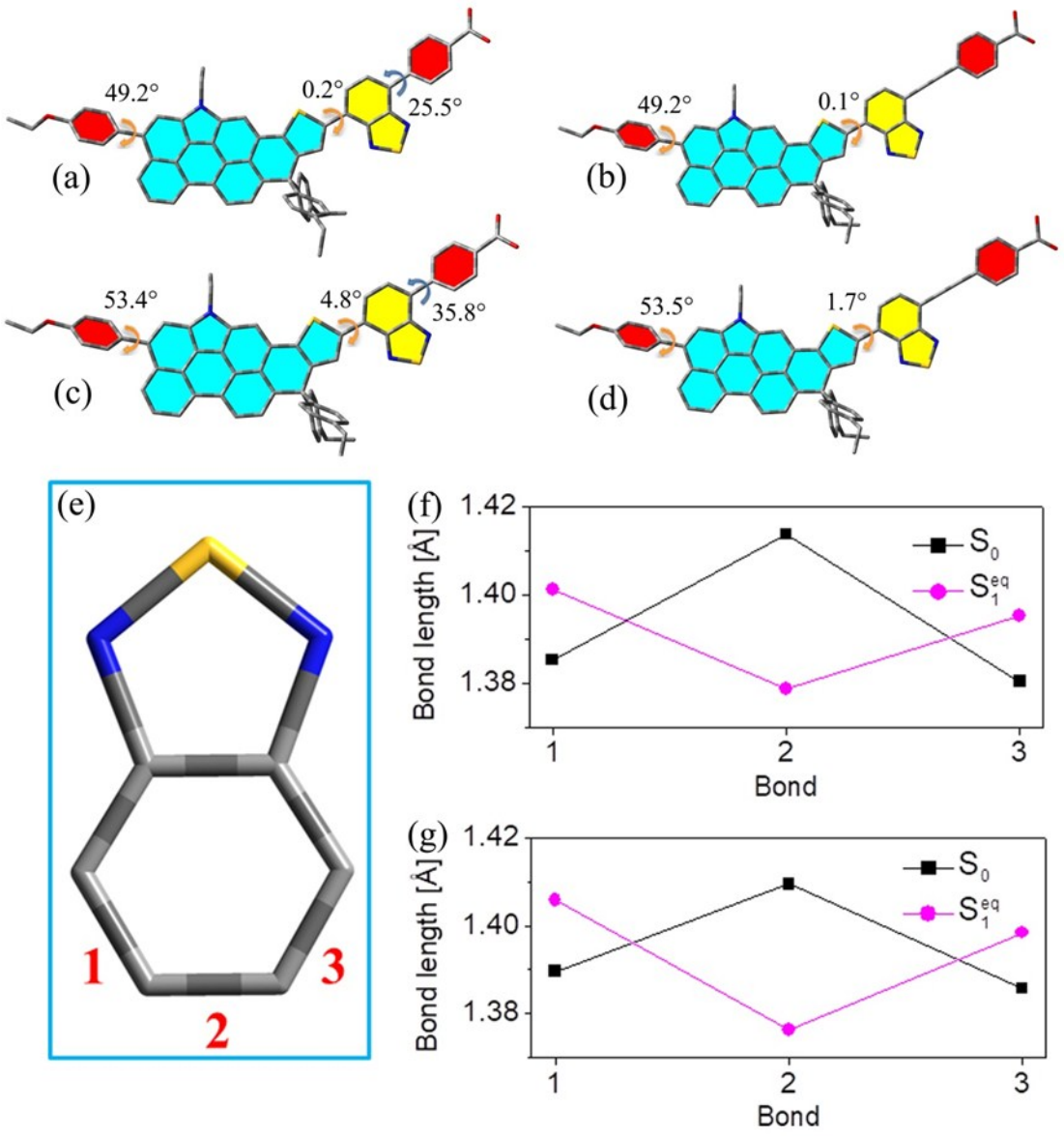


**Fig. S4** (a–d) Optimized geometries in PhMe of the $S_1^{eq}$ states: (a) C296; (b) C298, and the $S_0$ states: (c) C296; (d) C298. The large aliphatic chains were replaced with ethyl to improve the computational efficiency. Selected dihedral angles are shown near a molecular skeleton, and are evidently distinct at the $S_0$ and $S_1^{eq}$ states for C296 and C298. Aromatic units are filled with different colors for clarity of presentation. (e) Bonds 1, 2, and 3 of the benzo[*c*][1,2,5]thiadiazole (BT) unit. (f,g) Bond length alternations in the BT unit of dyes in PhMe at the $S_0$ and $S_1^{eq}$ states: (f) C296; (g) C298.

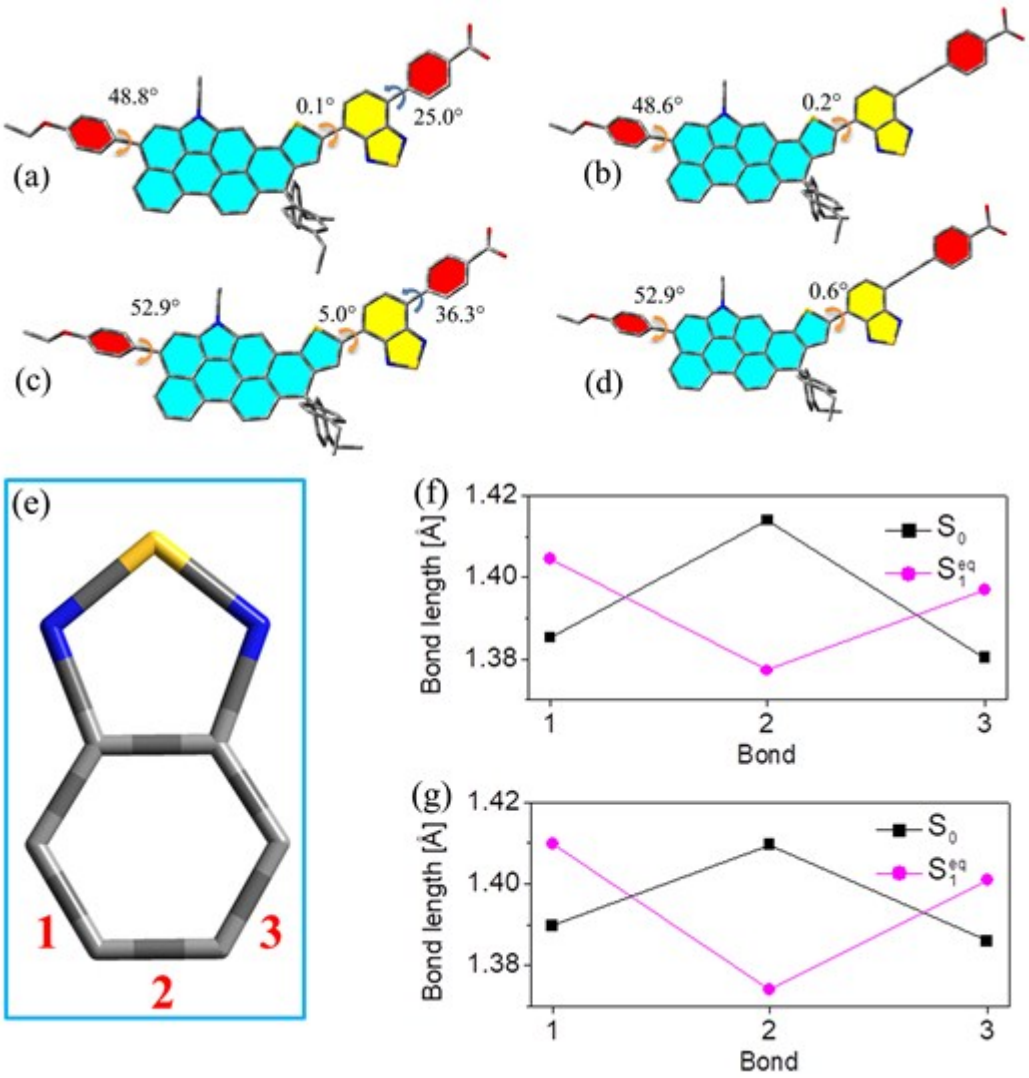


**Fig. S5** (a–d) Optimized geometries in THF of the $S_1^{eq}$ states: (a) C296; (b) C298, and the $S_0$ states: (c) C296; (d) C298. The large aliphatic chains were replaced with ethyl to improve the computational efficiency. Selected dihedral angles are shown near a molecular skeleton, and are evidently distinct at the $S_0$ and $S_1^{eq}$ states for C296 and C298. Aromatic units are filled with different colors for clarity of presentation. (e) Bonds 1, 2, and 3 of the benzo[*c*][1,2,5]thiadiazole (BT) unit. (f,g) Bond length alternations in the BT unit of dyes in THF at the $S_0$ and $S_1^{eq}$ states: (f) C296; (g) C298.

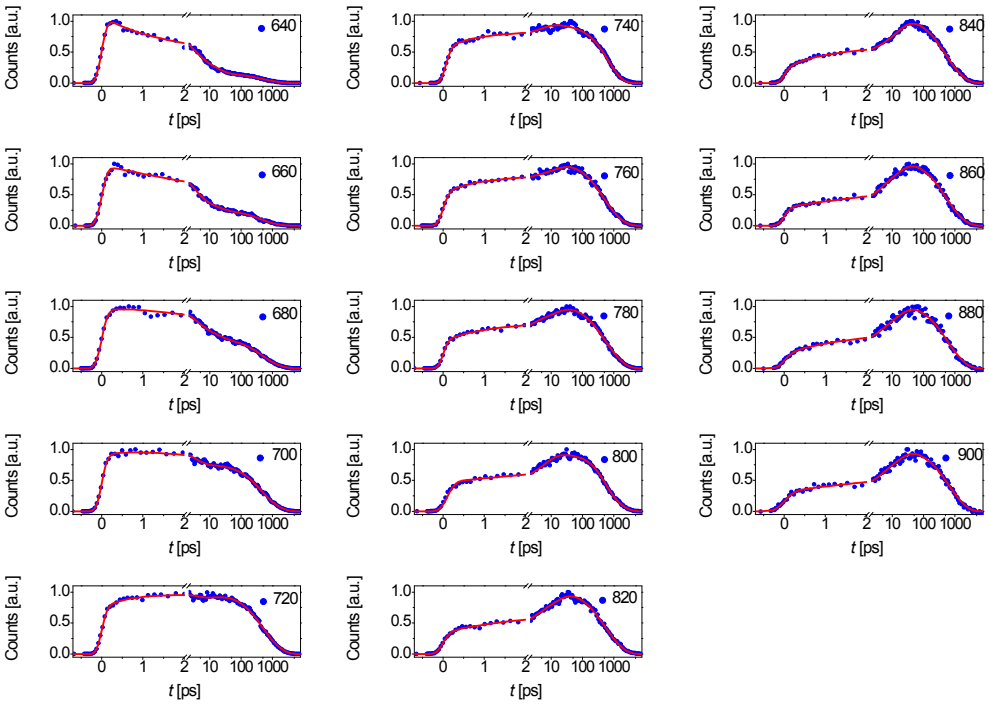


**Fig. S6** Normalized fluorescence traces (blue dots) probed at different wavelengths for C296 in PhMe (50 μM). The red solid lines are fittings via eqn.: $I_{\mathrm{FL}} \propto \sum_{i=1}^{n} A_i \exp(-t/\tau_i) \otimes \mathrm{IRF}$. Excitation wavelength: 530 nm.

**Table S2** Time constants and amplitudes used to fit fluorescence traces of C296 in PhMe

| $\lambda$ [nm] | $\tau_1$ [ps] | $A_1$ | $\tau_2$ [ps] | $A_2$ | $\tau_3$ [ps] | $A_3$ | $\tau_4$ [ps] | $A_4$ | $\tau_5$ [ps] | $A_5$ | $\bar{\tau}$ [ps] |
|---|---|---|---|---|---|---|---|---|---|---|---|
| 640 | 0.74 | 0.170 | 2.76 | 0.425 | 14.9 | 0.261 | 332 | 0.075 | 1120 | 0.069 | 107 |
| 660 | 0.74 | –0.088 | 2.76 | 0.510 | 14.9 | 0.210 | 332 | 0.172 | 1120 | 0.108 | 183 |
| 680 | 0.74 | –0.156 | 2.76 | 0.351 | 14.9 | 0.210 | 332 | 0.239 | 1120 | 0.200 | 307 |
| 700 | 0.74 | –0.195 | 2.76 | 0.327 | 14.9 | –0.018 | 332 | 0.385 | 1120 | 0.288 | 451 |
| 720 | 0.74 | –0.275 | 2.76 | 0.155 | 14.9 | –0.098 | 332 | 0.428 | 1120 | 0.417 | 609 |
| 740 | 0.74 | –0.274 | 2.76 | –0.410 | 14.9 | –0.314 | 332 | 0.474 | 1120 | 0.526 | 746 |
| 760 | 0.74 | –0.233 | 2.76 | –0.026 | 14.9 | –0.261 | 332 | 0.443 | 1120 | 0.557 | 771 |
| 780 | 0.74 | –0.154 | 2.76 | –0.142 | 14.9 | –0.281 | 332 | 0.443 | 1120 | 0.557 | 771 |
| 800 | 0.74 | –0.647 | 2.76 | –0.048 | 14.9 | –0.402 | 332 | 0.443 | 1120 | 0.557 | 771 |
| 820 | 0.74 | –0.059 | 2.76 | –0.214 | 14.9 | –0.405 | 332 | 0.443 | 1120 | 0.557 | 771 |
| 840 | 0.74 | –0.248 | 2.76 | –0.004 | 14.9 | –0.560 | 332 | 0.443 | 1120 | 0.557 | 771 |
| 860 | 0.74 | –0.016 | 2.76 | –0.252 | 14.9 | –0.508 | 332 | 0.443 | 1120 | 0.557 | 771 |
| 880 | 0.74 | –0.116 | 2.76 | –0.178 | 14.9 | –0.484 | 332 | 0.443 | 1120 | 0.557 | 771 |
| 900 | 0.74 | –0.018 | 2.76 | –0.211 | 14.9 | –0.490 | 332 | 0.443 | 1120 | 0.557 | 771 |

The average lifetime ($\bar{\tau}$) at a certain fluorescence wavelength was calculated with eqn.:

$$\bar{\tau} = \sum_{i=1}^{n} A_i \tau_i \Big/ \sum_{i=1}^{n} A_i \quad (A_i > 0) .$$

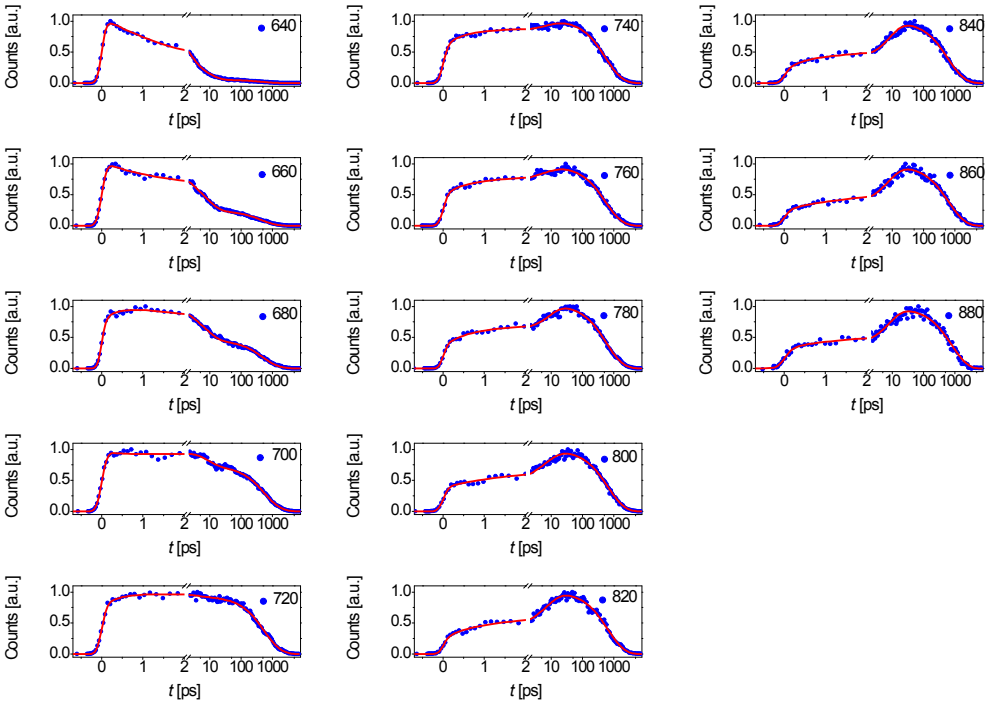


**Fig. S7** Normalized fluorescence traces (blue dots) probed at different wavelengths for C298 in PhMe (50 μM). The red solid lines are fittings via eqn.: $I_{\mathrm{FL}} \propto \sum_{i=1}^{n} A_i \exp(-t/\tau_i) \otimes \mathrm{IRF}$. Excitation wavelength: 530 nm.

**Table S3** Time constants and amplitudes used to fit fluorescence traces of C298 in PhMe

| $\lambda$ [nm] | $\tau_1$ [ps] | $A_1$ | $\tau_2$ [ps] | $A_2$ | $\tau_3$ [ps] | $A_3$ | $\tau_4$ [ps] | $A_4$ | $\tau_5$ [ps] | $A_5$ | $\bar{\tau}$ [ps] |
|---|---|---|---|---|---|---|---|---|---|---|---|
| 640 | 0.46 | –0.112 | 1.56 | 0.659 | 7.89 | 0.293 | 416 | 0.037 | 1070 | 0.011 | 30.4 |
| 660 | 0.46 | 0.076 | 1.56 | 0.154 | 7.89 | 0.538 | 416 | 0.198 | 1070 | 0.034 | 123 |
| 680 | 0.46 | –0.314 | 1.56 | 0.157 | 7.89 | 0.441 | 416 | 0.282 | 1070 | 0.120 | 250 |
| 700 | 0.46 | 0.100 | 1.56 | –0.159 | 7.89 | 0.273 | 416 | 0.357 | 1070 | 0.270 | 440 |
| 720 | 0.46 | –0.253 | 1.56 | 0.072 | 7.89 | 0.026 | 416 | 0.523 | 1070 | 0.379 | 624 |
| 740 | 0.46 | –0.275 | 1.56 | 0.024 | 7.89 | –0.180 | 416 | 0.540 | 1070 | 0.436 | 692 |
| 760 | 0.46 | –0.211 | 1.56 | –0.078 | 7.89 | –0.216 | 416 | 0.498 | 1070 | 0.502 | 744 |
| 780 | 0.46 | –0.780 | 1.56 | –0.264 | 7.89 | –0.537 | 416 | 0.498 | 1070 | 0.502 | 744 |
| 800 | 0.46 | –0.044 | 1.56 | –0.108 | 7.89 | –0.467 | 416 | 0.498 | 1070 | 0.502 | 744 |
| 820 | 0.46 | –0.154 | 1.56 | –0.047 | 7.89 | –0.532 | 416 | 0.498 | 1070 | 0.502 | 744 |
| 840 | 0.46 | –0.255 | 1.56 | –0.145 | 7.89 | –0.701 | 416 | 0.498 | 1070 | 0.502 | 744 |
| 860 | 0.46 | –0.077 | 1.56 | –0.019 | 7.89 | –0.618 | 416 | 0.498 | 1070 | 0.502 | 744 |
| 880 | 0.46 | –0.137 | 1.56 | –0.091 | 7.89 | –0.659 | 416 | 0.498 | 1070 | 0.502 | 744 |

The average lifetime ($\bar{\tau}$) at a certain fluorescence wavelength was calculated with eqn.:

$$\bar{\tau} = \sum_{i=1}^{n} A_i \tau_i \Big/ \sum_{i=1}^{n} A_i \quad (A_i > 0) .$$

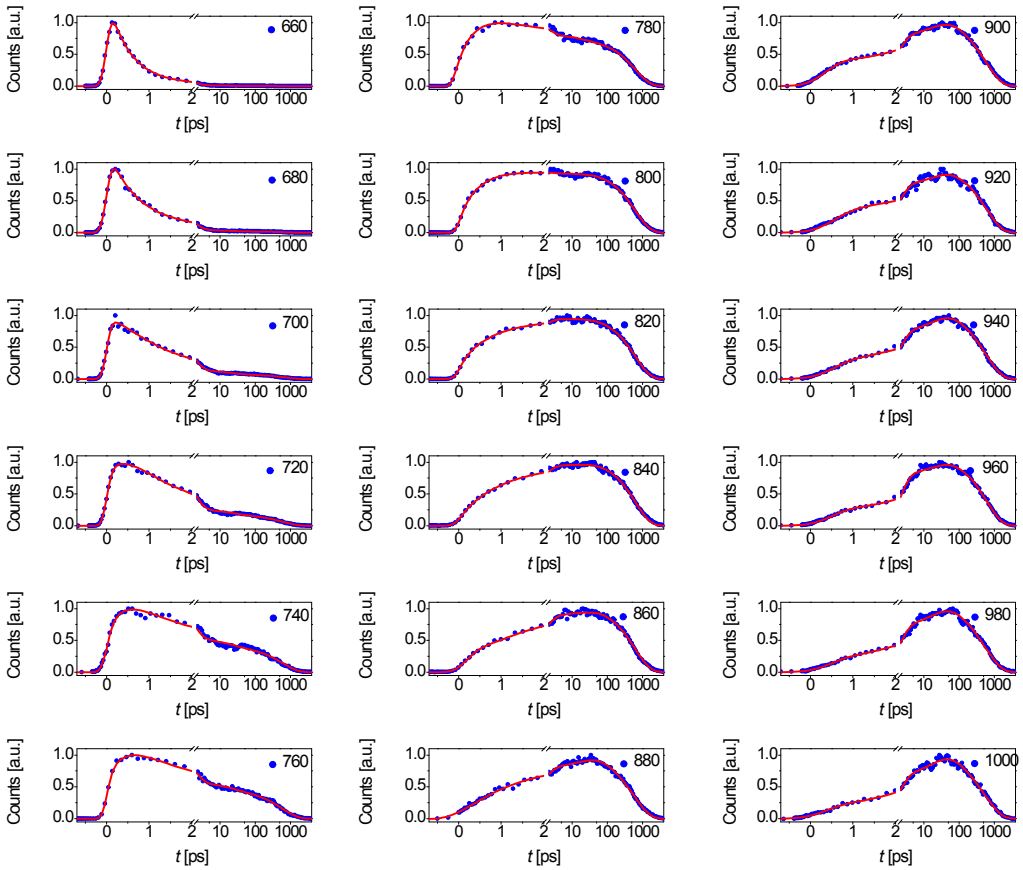


**Fig. S8** Normalized fluorescence traces (blue dots) probed at different wavelengths for C296 in THF (50 μM). The red solid lines are fittings via eqn.: $I_{\mathrm{FL}} \propto \sum_{i=1}^{n} A_i \exp(-t/\tau_i) \otimes \mathrm{IRF}$. Excitation wavelength: 530 nm.

**Table S4** Time constants and amplitudes used to fit fluorescence traces of C296 in THF

| $\lambda$ [nm] | $\tau_1$ [ps] | $A_1$ | $\tau_2$ [ps] | $A_2$ | $\tau_3$ [ps] | $A_3$ | $\tau_4$ [ps] | $A_4$ | $\tau_5$ [ps] | $A_5$ | $\bar{\tau}$ [ps] |
|---|---|---|---|---|---|---|---|---|---|---|---|
| 660 | 0.45 | 0.803 | 1.03 | 0.185 | 21.6 | 0.007 | 126 | –0.002 | 619 | 0.005 | 3.60 |
| 680 | 0.45 | 0.394 | 1.03 | 0.576 | 21.6 | 0.017 | 126 | –0.003 | 619 | 0.013 | 9.07 |
| 700 | 0.45 | –0.374 | 1.03 | 0.918 | 21.6 | 0.046 | 126 | –0.006 | 619 | 0.036 | 24.4 |
| 720 | 0.45 | –0.647 | 1.03 | 0.877 | 21.6 | 0.039 | 126 | 0.004 | 619 | 0.080 | 51.6 |
| 740 | 0.45 | –0.719 | 1.03 | 0.737 | 21.6 | 0.063 | 126 | 0.012 | 619 | 0.188 | 120 |
| 760 | 0.45 | –0.064 | 1.03 | 0.565 | 21.6 | 0.089 | 126 | 0.030 | 619 | 0.316 | 202 |
| 780 | 0.45 | –0.197 | 1.03 | –0.118 | 21.6 | 0.367 | 126 | 0.064 | 619 | 0.569 | 368 |
| 800 | 0.45 | –0.971 | 1.03 | –0.172 | 21.6 | –0.033 | 126 | 0.255 | 619 | 0.745 | 493 |
| 820 | 0.45 | –0.269 | 1.03 | –0.439 | 21.6 | –0.035 | 126 | 0.149 | 619 | 0.851 | 545 |
| 840 | 0.45 | –0.051 | 1.03 | –0.855 | 21.6 | –0.085 | 126 | 0.149 | 619 | 0.851 | 545 |
| 860 | 0.45 | –0.107 | 1.03 | –0.552 | 21.6 | –0.169 | 126 | 0.149 | 619 | 0.851 | 545 |
| 880 | 0.45 | –0.326 | 1.03 | –0.123 | 21.6 | –0.255 | 126 | 0.149 | 619 | 0.851 | 545 |
| 900 | 0.45 | –0.216 | 1.03 | –0.228 | 21.6 | –0.305 | 126 | 0.149 | 619 | 0.851 | 545 |
| 920 | 0.45 | –0.810 | 1.03 | –0.637 | 21.6 | –0.287 | 126 | 0.149 | 619 | 0.851 | 545 |
| 940 | 0.45 | –0.553 | 1.03 | –0.200 | 21.6 | –0.325 | 126 | 0.149 | 619 | 0.851 | 545 |
| 960 | 0.45 | –0.186 | 1.03 | –0.153 | 21.6 | –0.379 | 126 | 0.149 | 619 | 0.851 | 545 |
| 980 | 0.45 | –0.173 | 1.03 | –0.331 | 21.6 | –0.357 | 126 | 0.149 | 619 | 0.851 | 545 |
| 1000 | 0.45 | –0.533 | 1.03 | –0.418 | 21.6 | –0.358 | 126 | 0.149 | 619 | 0.851 | 545 |

The average lifetime ($\bar{\tau}$) at a certain fluorescence wavelength was calculated with eqn.:

$$\bar{\tau} = \sum_{i=1}^{n} A_i \tau_i \Big/ \sum_{i=1}^{n} A_i \quad (A_i > 0) .$$

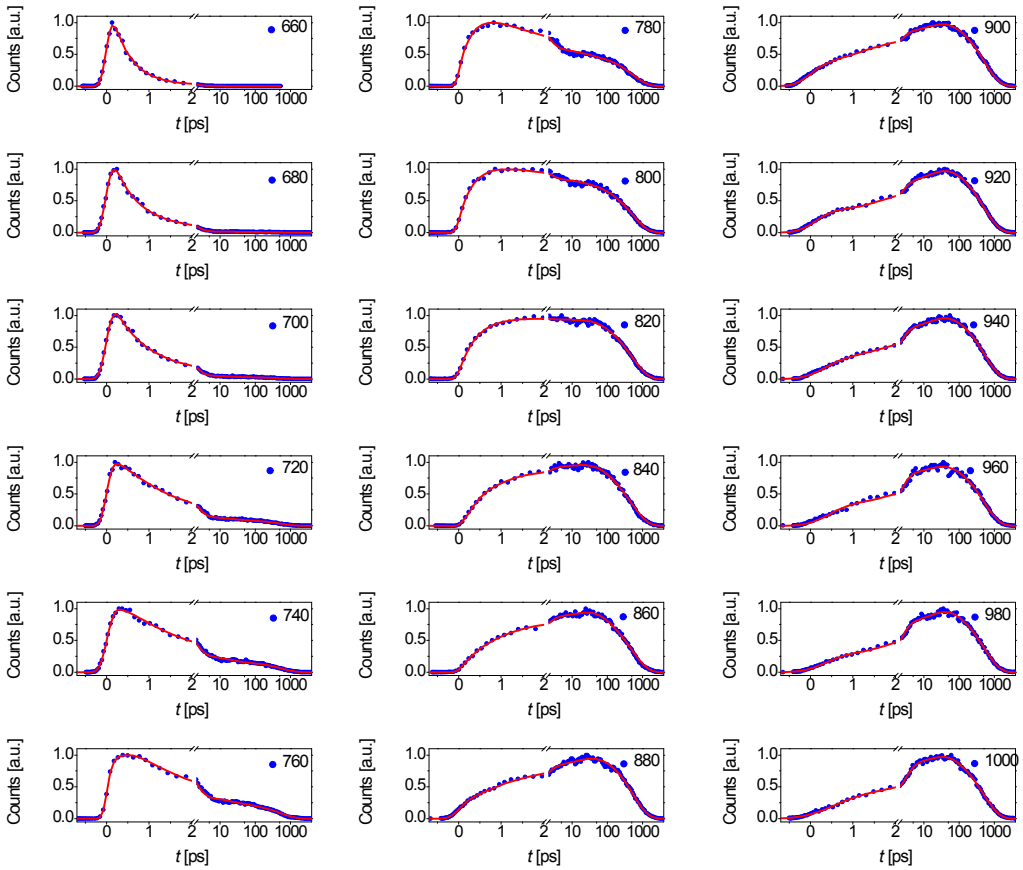


**Fig. S9** Normalized fluorescence traces (blue dots) probed at different wavelengths for C298 in THF (50 μM). The red solid lines are fittings via eqn.: $I_{\mathrm{FL}} \propto \sum_{i=1}^{n} A_i \exp(-t/\tau_i) \otimes \mathrm{IRF}$. Excitation wavelength: 530 nm.

**Table S5** Time constants and amplitudes used to fit fluorescence traces of C298 in THF

| $\lambda$ [nm] | $\tau_1$ [ps] | $A_1$ | $\tau_2$ [ps] | $A_2$ | $\tau_3$ [ps] | $A_3$ | $\tau_4$ [ps] | $A_4$ | $\tau_5$ [ps] | $A_5$ | $\bar{\tau}$ [ps] |
|---|---|---|---|---|---|---|---|---|---|---|---|
| 660 | 0.43 | 0.925 | 1.09 | 0.068 | 18.5 | 0.005 | 106 | –0.002 | 533 | 0.002 | 1.53 |
| 680 | 0.43 | 0.613 | 1.09 | 0.374 | 18.5 | 0.005 | 106 | 0.001 | 533 | 0.007 | 4.75 |
| 700 | 0.43 | 0.306 | 1.09 | 0.655 | 18.5 | 0.016 | 106 | 0 | 533 | 0.023 | 13.4 |
| 720 | 0.43 | –0.319 | 1.09 | 0.910 | 18.5 | 0.038 | 106 | –0.001 | 533 | 0.052 | 29.6 |
| 740 | 0.43 | –0.050 | 1.09 | 0.832 | 18.5 | 0.068 | 106 | –0.008 | 533 | 0.100 | 55.5 |
| 760 | 0.43 | –0.434 | 1.09 | 0.715 | 18.5 | 0.084 | 106 | 0.013 | 533 | 0.188 | 104 |
| 780 | 0.43 | –0.483 | 1.09 | 0.527 | 18.5 | 0.104 | 106 | 0.023 | 533 | 0.346 | 189 |
| 800 | 0.43 | –0.284 | 1.09 | 0.364 | 18.5 | 0.036 | 106 | 0.042 | 533 | 0.558 | 303 |
| 820 | 0.43 | –0.367 | 1.09 | 0.136 | 18.5 | –0.063 | 106 | 0.092 | 533 | 0.772 | 422 |
| 840 | 0.43 | –0.564 | 1.09 | –0.429 | 18.5 | –0.149 | 106 | 0.171 | 533 | 0.829 | 460 |
| 860 | 0.43 | –0.124 | 1.09 | –0.662 | 18.5 | –0.208 | 106 | 0.171 | 533 | 0.829 | 460 |
| 880 | 0.43 | –0.237 | 1.09 | –0.712 | 18.5 | –0.194 | 106 | 0.171 | 533 | 0.829 | 460 |
| 900 | 0.43 | –0.098 | 1.09 | –0.203 | 18.5 | –0.241 | 106 | 0.171 | 533 | 0.829 | 460 |
| 920 | 0.43 | –0.196 | 1.09 | –0.081 | 18.5 | –0.337 | 106 | 0.171 | 533 | 0.829 | 460 |
| 940 | 0.43 | –0.531 | 1.09 | –0.364 | 18.5 | –0.254 | 106 | 0.171 | 533 | 0.829 | 460 |
| 960 | 0.43 | –0.629 | 1.09 | –0.204 | 18.5 | –0.216 | 106 | 0.171 | 533 | 0.829 | 460 |
| 980 | 0.43 | –0.744 | 1.09 | –0.303 | 18.5 | –0.290 | 106 | 0.171 | 533 | 0.829 | 460 |
| 1000 | 0.43 | –0.175 | 1.09 | –0.107 | 18.5 | –0.282 | 106 | 0.171 | 533 | 0.829 | 460 |

The average lifetime ($\bar{\tau}$) at a certain fluorescence wavelength was calculated with eqn.:

$$\bar{\tau} = \sum_{i=1}^{n} A_i \tau_i \,/\, \sum_{i=1}^{n} A_i \quad (A_i > 0) \,.$$

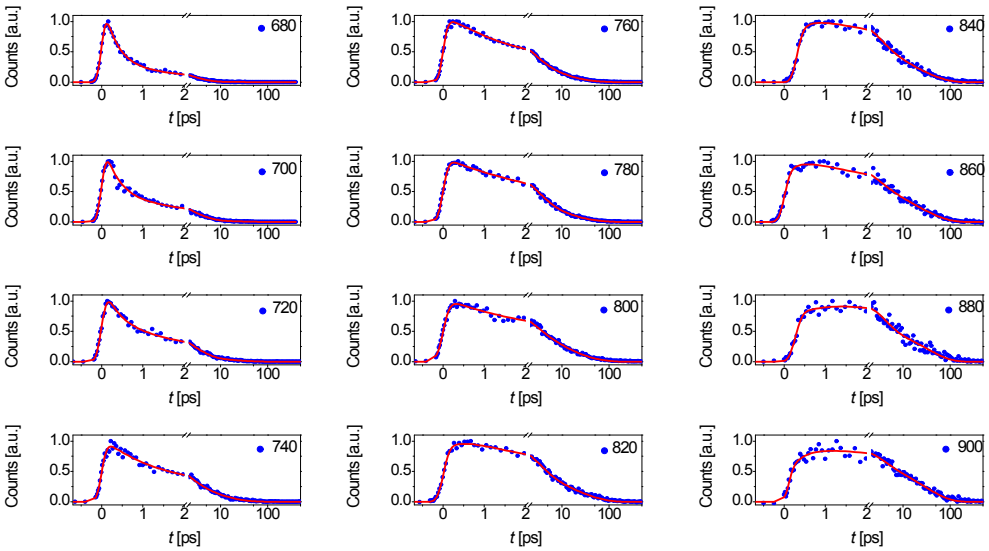


**Fig. S10** Normalized kinetic traces (blue dots) at a series of fluorescence wavelengths for the C296-grafted titania film in contact with a Co-bpy redox electrolyte. The red solid lines are fittings via eqn.: $I_{\mathrm{FL}} \propto \sum_{i=1}^{n} A_i \exp(-t/\tau_i) \otimes \mathrm{IRF}$. Excitation wavelength: 530 nm.

**Table S6** Time constants and amplitudes used to fit fluorescence traces of the C296-grafted titania film in contact with a Co-bpy redox electrolyte

| $\lambda$ [nm] | $\tau_1$ [ps] | $A_1$ | $\tau_2$ [ps] | $A_2$ | $\tau_3$ [ps] | $A_3$ | $\tau_4$ [ps] | $A_4$ | $\tau_5$ [ps] | $A_5$ | $\bar{\tau}$ [ps] |
|---|---|---|---|---|---|---|---|---|---|---|---|
| 680 | 0.31 | 0.712 | 0.83 | 0.133 | 2.69 | 0.149 | 11.5 | –0.005 | 41.3 | 0.006 | 1.31 |
| 700 | 0.31 | 0.602 | 0.83 | 0.125 | 2.69 | 0.254 | 11.5 | 0.009 | 41.3 | 0.010 | 1.94 |
| 720 | 0.31 | 0.397 | 0.83 | 0.189 | 2.69 | 0.356 | 11.5 | 0.039 | 41.3 | 0.019 | 3.04 |
| 740 | 0.31 | –0.122 | 0.83 | 0.482 | 2.69 | 0.331 | 11.5 | 0.166 | 41.3 | 0.021 | 4.73 |
| 760 | 0.31 | –0.214 | 0.83 | 0.339 | 2.69 | 0.446 | 11.5 | 0.167 | 41.3 | 0.048 | 5.96 |
| 780 | 0.31 | –0.030 | 0.83 | 0.009 | 2.69 | 0.688 | 11.5 | 0.217 | 41.3 | 0.086 | 8.51 |
| 800 | 0.31 | –0.064 | 0.83 | 0.075 | 2.69 | 0.473 | 11.5 | 0.291 | 41.3 | 0.161 | 11.9 |
| 820 | 0.31 | –0.182 | 0.83 | –0.148 | 2.69 | 0.573 | 11.5 | 0.182 | 41.3 | 0.245 | 14.3 |
| 840 | 0.31 | –0.226 | 0.83 | –0.184 | 2.69 | 0.480 | 11.5 | 0.208 | 41.3 | 0.312 | 17.2 |
| 860 | 0.31 | –0.414 | 0.83 | –0.051 | 2.69 | 0.443 | 11.5 | 0.233 | 41.3 | 0.324 | 17.9 |
| 880 | 0.31 | –0.182 | 0.83 | –0.634 | 2.69 | 0.443 | 11.5 | 0.233 | 41.3 | 0.324 | 17.9 |
| 900 | 0.31 | –0.254 | 0.83 | –0.275 | 2.69 | 0.443 | 11.5 | 0.233 | 41.3 | 0.324 | 17.9 |

The average lifetime ($\bar{\tau}$) at a certain fluorescence wavelength was calculated with eqn.: $\bar{\tau} = \sum_{i=1}^{n} A_i \tau_i / \sum_{i=1}^{n} A_i \ (A_i > 0)$.

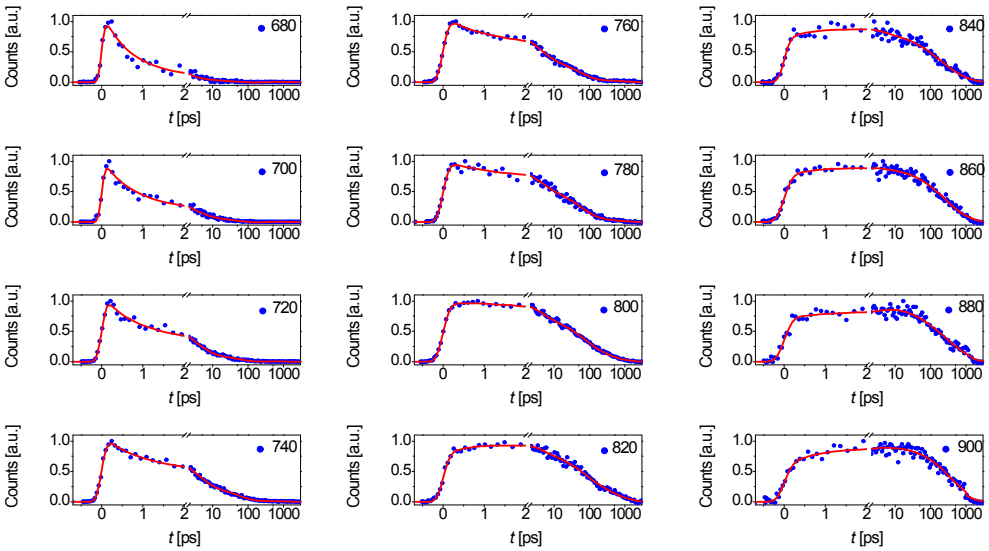


**Fig. S11** Normalized kinetic traces (blue dots) at a series of fluorescence wavelengths for the C296-grafted alumina film in contact with a Co-bpy redox electrolyte. The red solid lines are fittings via eqn.: $I_{\mathrm{FL}} \propto \sum_{i=1}^{n} A_i \exp(-t/\tau_i) \otimes \mathrm{IRF}$. Excitation wavelength: 530 nm.

**Table S7** Time constants and amplitudes used to fit fluorescence traces of the C296-grafted alumina film in contact with a Co-bpy redox electrolyte

| $\lambda$ [nm] | $\tau_1$ [ps] | $A_1$ | $\tau_2$ [ps] | $A_2$ | $\tau_3$ [ps] | $A_3$ | $\tau_4$ [ps] | $A_4$ | $\tau_5$ [ps] | $A_5$ | $\bar{\tau}$ [ps] |
|---|---|---|---|---|---|---|---|---|---|---|---|
| 680 | 0.72 | 0.868 | 4.31 | 0.081 | 55.6 | 0.051 | 235 | –0.029 | 918 | –0.012 | 3.82 |
| 700 | 0.72 | 0.672 | 4.31 | 0.231 | 55.6 | 0.097 | 235 | –0.038 | 918 | –0.013 | 6.87 |
| 720 | 0.72 | 0.392 | 4.31 | 0.396 | 55.6 | 0.212 | 235 | –0.019 | 918 | –0.011 | 13.8 |
| 740 | 0.72 | 0.319 | 4.31 | 0.439 | 55.6 | 0.224 | 235 | –0.013 | 918 | 0.018 | 31.1 |
| 760 | 0.72 | 0.207 | 4.31 | 0.436 | 55.6 | 0.318 | 235 | –0.005 | 918 | 0.039 | 55.9 |
| 780 | 0.72 | –0.105 | 4.31 | 0.213 | 55.6 | 0.624 | 235 | 0.103 | 918 | 0.060 | 115 |
| 800 | 0.72 | –0.161 | 4.31 | –0.473 | 55.6 | 0.525 | 235 | 0.351 | 918 | 0.124 | 225 |
| 820 | 0.72 | –0.914 | 4.31 | –0.766 | 55.6 | –0.605 | 235 | 0.772 | 918 | 0.228 | 391 |
| 840 | 0.72 | –0.398 | 4.31 | –0.238 | 55.6 | –0.320 | 235 | 0.678 | 918 | 0.322 | 455 |
| 860 | 0.72 | –0.238 | 4.31 | –0.049 | 55.6 | –0.169 | 235 | 0.625 | 918 | 0.375 | 491 |
| 880 | 0.72 | –0.120 | 4.31 | –0.176 | 55.6 | –0.257 | 235 | 0.625 | 918 | 0.375 | 491 |
| 900 | 0.72 | –0.364 | 4.31 | –0.042 | 55.6 | –0.051 | 235 | 0.625 | 918 | 0.375 | 491 |

The average lifetime ($\bar{\tau}$) at a certain fluorescence wavelength was calculated with eqn.: $\bar{\tau} = \sum_{i=1}^{n} A_i \tau_i / \sum_{i=1}^{n} A_i \ (A_i > 0)$.

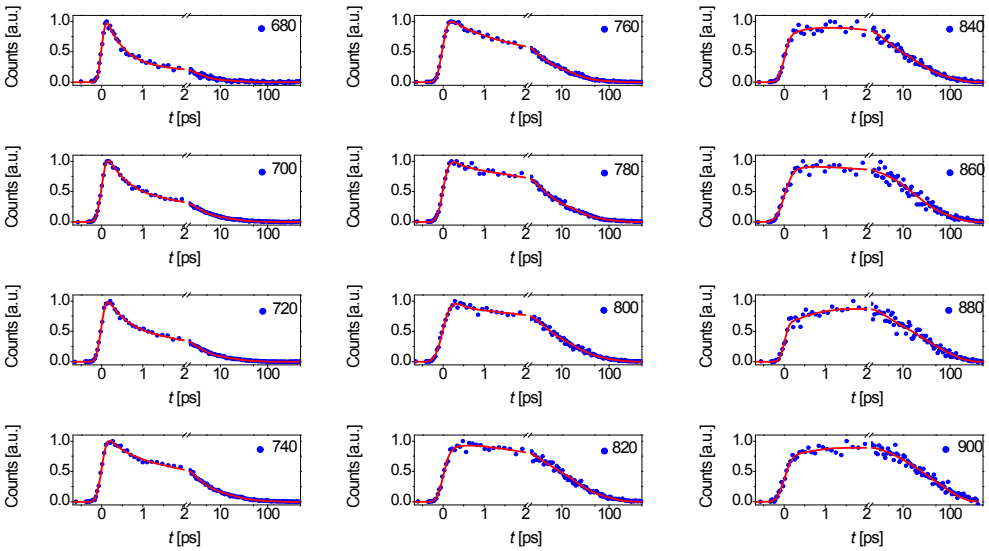


**Fig. S12** Normalized kinetic traces (blue dots) at a series of fluorescence wavelengths for the C298-grafted titania film in contact with a Co-bpy redox electrolyte. The red solid lines are fittings via eqn.: $I_{\mathrm{FL}} \propto \sum_{i=1}^{n} A_i \exp(-t/\tau_i) \otimes \mathrm{IRF}$. Excitation wavelength: 530 nm.

**Table S8** Time constants and amplitudes used to fit fluorescence traces of the C298-grafted titania film in contact with a Co-bpy redox electrolyte

| $\lambda$ [nm] | $\tau_1$ [ps] | $A_1$ | $\tau_2$ [ps] | $A_2$ | $\tau_3$ [ps] | $A_3$ | $\tau_4$ [ps] | $A_4$ | $\tau_5$ [ps] | $A_5$ | $\bar{\tau}$ [ps] |
|---|---|---|---|---|---|---|---|---|---|---|---|
| 680 | 0.43 | 0.560 | 0.89 | 0.193 | 2.03 | 0.234 | 15.1 | 0.013 | 80.6 | –0.004 | 1.08 |
| 700 | 0.43 | 0.554 | 0.89 | –0.129 | 2.03 | 0.383 | 15.1 | 0.063 | 80.6 | –0.009 | 1.96 |
| 720 | 0.43 | 0.494 | 0.89 | –0.152 | 2.03 | 0.404 | 15.1 | 0.094 | 80.6 | 0.009 | 3.14 |
| 740 | 0.43 | 0.328 | 0.89 | –0.289 | 2.03 | 0.519 | 15.1 | 0.132 | 80.6 | 0.021 | 4.87 |
| 760 | 0.43 | 0.110 | 0.89 | –0.077 | 2.03 | 0.624 | 15.1 | 0.225 | 80.6 | 0.041 | 8.01 |
| 780 | 0.43 | –0.377 | 0.89 | –0.593 | 2.03 | 0.679 | 15.1 | 0.245 | 80.6 | 0.076 | 11.2 |
| 800 | 0.43 | –0.580 | 0.89 | –0.760 | 2.03 | 0.555 | 15.1 | 0.323 | 80.6 | 0.122 | 15.9 |
| 820 | 0.43 | –0.311 | 0.89 | –0.055 | 2.03 | 0.381 | 15.1 | 0.437 | 80.6 | 0.182 | 22.0 |
| 840 | 0.43 | –0.086 | 0.89 | –0.504 | 2.03 | –0.931 | 15.1 | 0.761 | 80.6 | 0.239 | 30.7 |
| 860 | 0.43 | –0.237 | 0.89 | –0.075 | 2.03 | –0.020 | 15.1 | 0.658 | 80.6 | 0.342 | 37.5 |
| 880 | 0.43 | –0.303 | 0.89 | –0.461 | 2.03 | –0.697 | 15.1 | 0.658 | 80.6 | 0.342 | 37.5 |
| 900 | 0.43 | –0.120 | 0.89 | –0.711 | 2.03 | –0.303 | 15.1 | 0.658 | 80.6 | 0.342 | 37.5 |

The average lifetime ($\bar{\tau}$) at a certain fluorescence wavelength was calculated with eqn.: $\bar{\tau} = \sum_{i=1}^{n} A_i \tau_i / \sum_{i=1}^{n} A_i \ (A_i > 0)$.

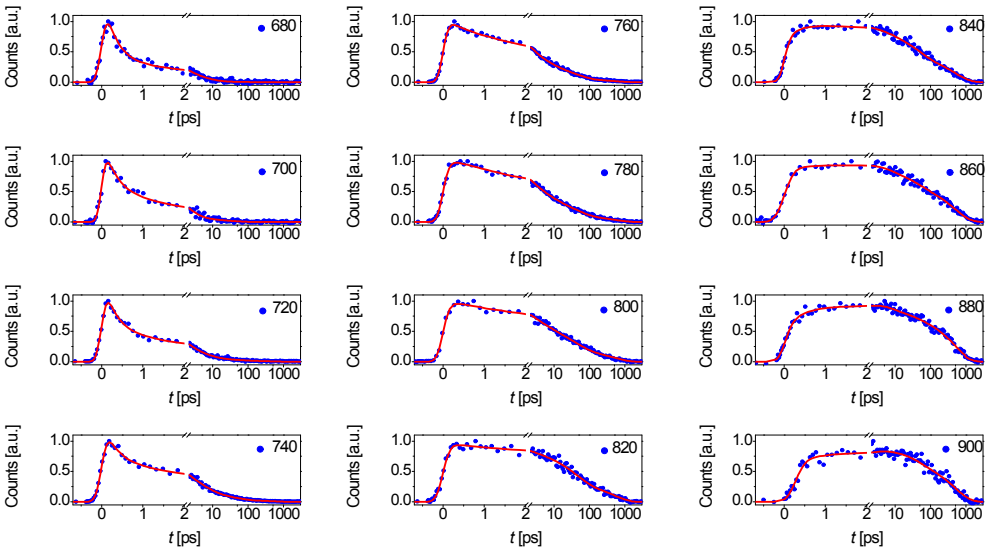


**Fig. S13** Normalized kinetic traces (blue dots) at a series of fluorescence wavelengths for the C298-grafted alumina film in contact with a Co-bpy redox electrolyte. The red solid lines are fittings via eqn.: $I_{\mathrm{FL}} \propto \sum_{i=1}^{n} A_i \exp(-t/\tau_i) \otimes \mathrm{IRF}$. Excitation wavelength: 530 nm.

**Table S9** Time constants and amplitudes used to fit fluorescence traces of the C298-grafted alumina film in contact with a Co-bpy redox electrolyte

| $\lambda$ [nm] | $\tau_1$ [ps] | $A_1$ | $\tau_2$ [ps] | $A_2$ | $\tau_3$ [ps] | $A_3$ | $\tau_4$ [ps] | $A_4$ | $\tau_5$ [ps] | $A_5$ | $\bar{\tau}$ [ps] |
|---|---|---|---|---|---|---|---|---|---|---|---|
| 680 | 0.28 | 0.747 | 1.58 | 0.153 | 6.56 | 0.091 | 44.1 | 0.007 | 496 | 0.002 | 2.31 |
| 700 | 0.28 | 0.560 | 1.58 | 0.353 | 6.56 | 0.054 | 44.1 | 0.028 | 496 | 0.005 | 4.92 |
| 720 | 0.28 | 0.602 | 1.58 | 0.229 | 6.56 | 0.123 | 44.1 | 0.033 | 496 | 0.013 | 9.16 |
| 740 | 0.28 | 0.483 | 1.58 | 0.206 | 6.56 | 0.210 | 44.1 | 0.078 | 496 | 0.023 | 16.9 |
| 760 | 0.28 | –0.018 | 1.58 | 0.485 | 6.56 | 0.253 | 44.1 | 0.217 | 496 | 0.045 | 34.2 |
| 780 | 0.28 | –0.150 | 1.58 | 0.394 | 6.56 | 0.262 | 44.1 | 0.253 | 496 | 0.091 | 58.4 |
| 800 | 0.28 | –0.103 | 1.58 | 0.248 | 6.56 | 0.230 | 44.1 | 0.343 | 496 | 0.179 | 106 |
| 820 | 0.28 | –0.010 | 1.58 | –0.127 | 6.56 | 0.118 | 44.1 | 0.542 | 496 | 0.340 | 193 |
| 840 | 0.28 | –0.470 | 1.58 | –0.027 | 6.56 | –0.168 | 44.1 | 0.401 | 496 | 0.599 | 315 |
| 860 | 0.28 | –0.135 | 1.58 | –0.115 | 6.56 | –0.195 | 44.1 | 0.248 | 496 | 0.752 | 384 |
| 880 | 0.28 | –0.509 | 1.58 | –0.230 | 6.56 | –0.186 | 44.1 | 0.248 | 496 | 0.752 | 384 |
| 900 | 0.28 | –0.176 | 1.58 | –0.125 | 6.56 | –0.026 | 44.1 | 0.248 | 496 | 0.752 | 384 |

The average lifetime ($\bar{\tau}$) at a certain fluorescence wavelength was calculated with eqn.: $\bar{\tau} = \sum_{i=1}^{n} A_i \tau_i / \sum_{i=1}^{n} A_i \ (A_i > 0)$.

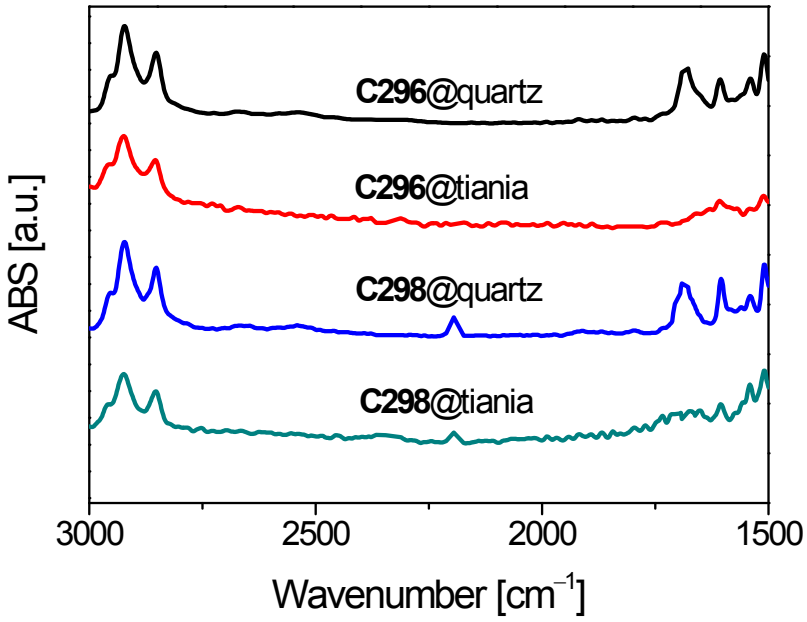


**Fig. S14** ATR-FTIR spectra of thin films with dyes C296 and C298. A strong vibrational peak of carboxylic acid (COOH) at 1686±3 $cm^{-1}$ was identified for C296 and C298 deposited on quartz. The absence of COOH signal for dyed titania films eliminated the possibility of physical adsorption of dye molecules on the surface of titania. The saturated aliphatic chains were clearly identified for their C–H stretch modes in the 2800–3000 $cm^{-1}$ region. Sharp peaks at 2853±3 and 2923±2 $cm^{-1}$ were ascribed to the symmetric and asymmetric $–CH_2–$ stretch vibrations. In addition, the corresponding $–CH_3$ peaks were probed at 2953±2 $cm^{-1}$. The triple bond for dye C298 was not influenced during the dye adsorption process by looking at the characteristic peak at 2195 $cm^{-1}$.

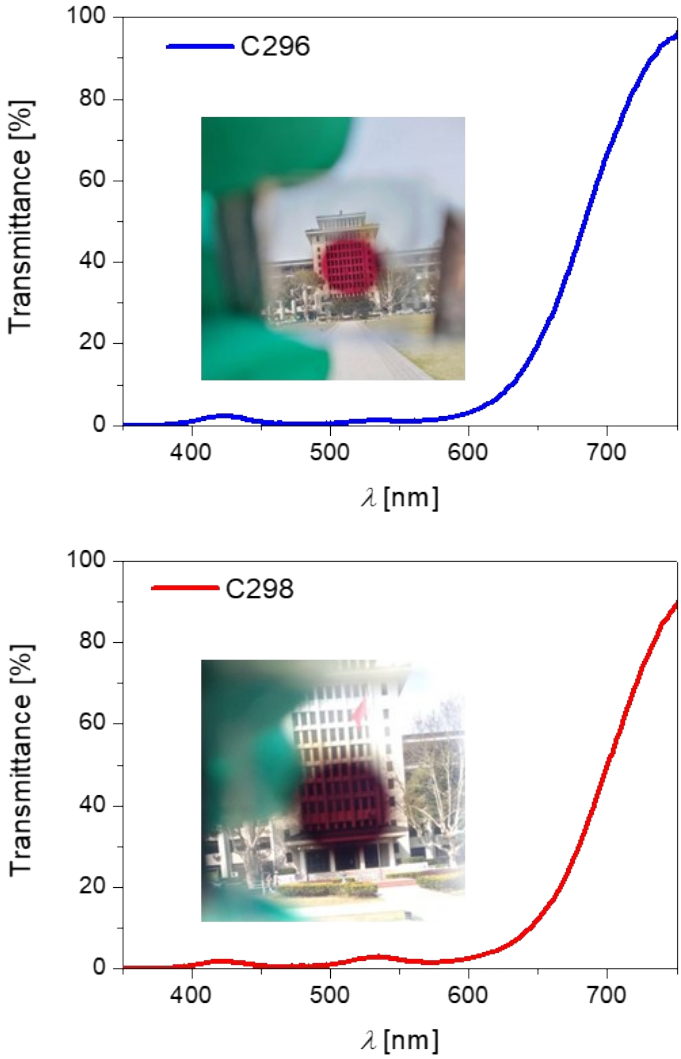


**Fig. S15** Transmittance spectra and photos of transparent DSSCs with C296 and C298.

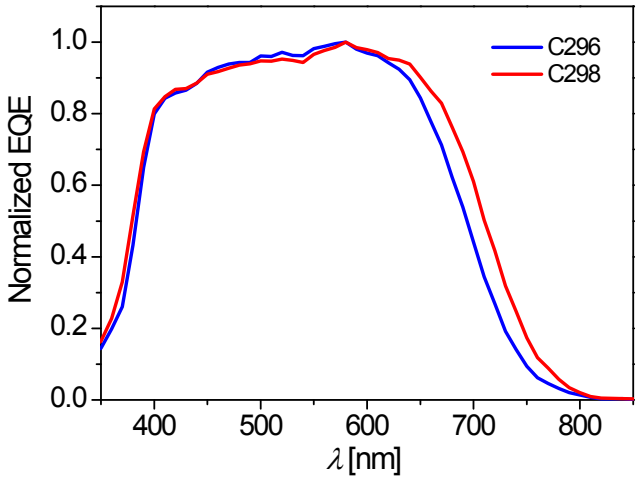


**Fig. S16** Plots of normalized external quantum efficiency (EQE) as a function of wavelength ( $\lambda$ ) of the fresh cells with C296 and C298.

**Table S10** Photovoltaic parameters of fresh cells without or with scattering layer measured under the AM1.5G conditions.

| Device | Scattering layer | $J_{SC}$ [mA cm$^{-2}$] | $V_{OC}$ [mV] | FF [%] | PCE [%] |
|---|---|---|---|---|---|
| C296 | without | 16.87 | 811 | 73.7 | 10.1 |
| C296 | with | 18.16 | 798 | 76.0 | 11.0 |
| C298 | without | 16.84 | 819 | 74.9 | 10.3 |
| C298 | with | 19.23 | 832 | 73.9 | 11.8 |

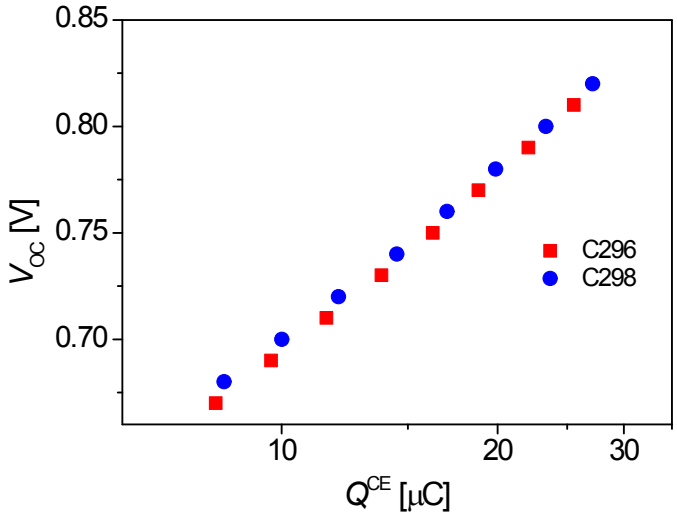


**Fig. S17** Plots of charges ( $Q^{CE}$ ) extracted from dye-grafted titania films as a function of open-circuit photovoltage ( $V_{oc}$ ) for the fresh cells with C296 and C298.

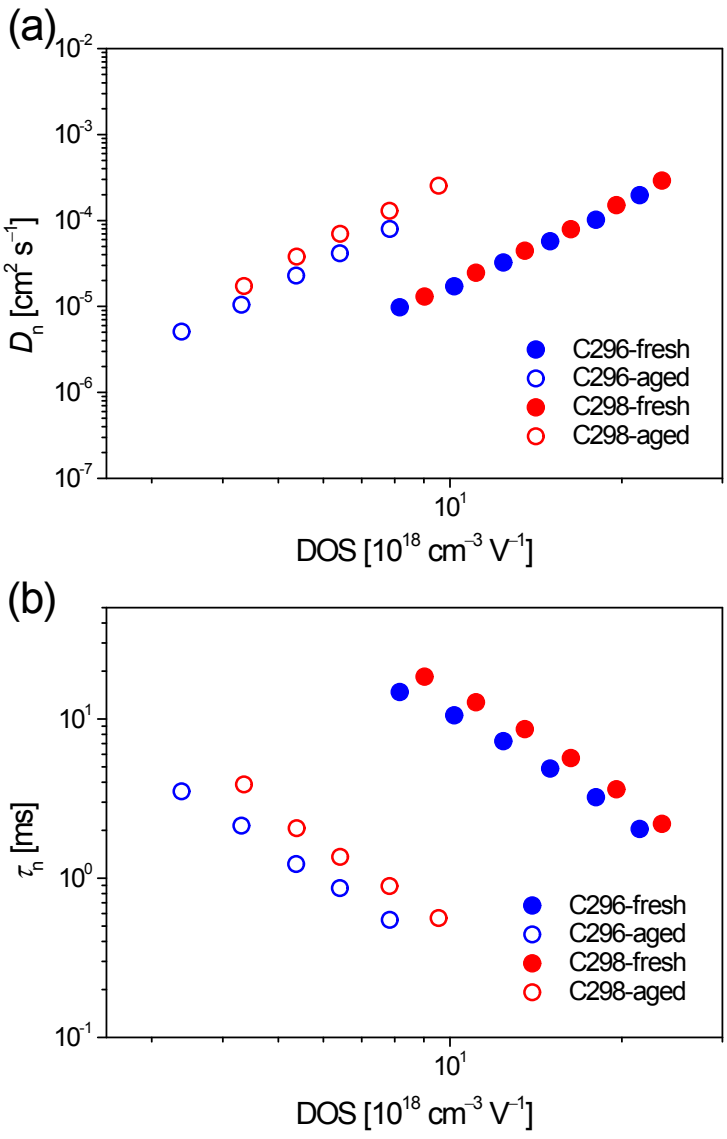


**Fig. S18** (a) Plots of electron diffusion coefficient ( $D_n$ ) as a function of density of states (DOS). (b) Plots of electron lifetime ( $\tau_n$ ) as a function of DOS. The data were derived from impedance spectra. Note that $L_n$ is equal to $\sqrt{D_n \tau_n}$ .

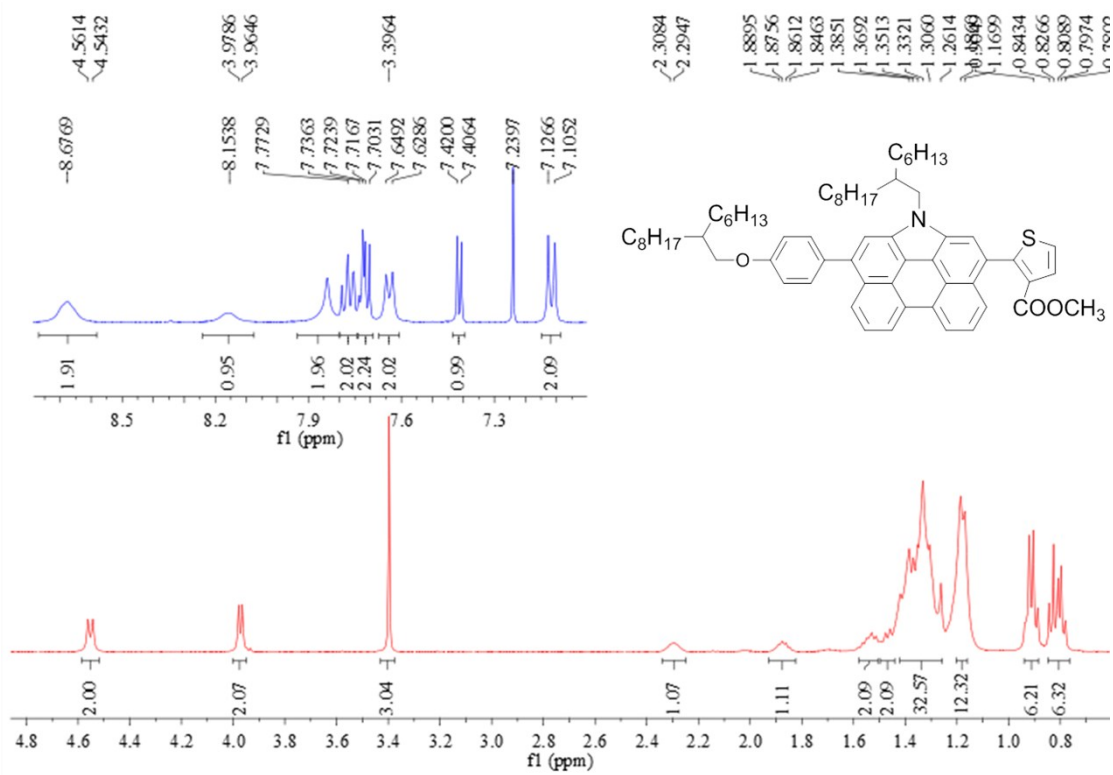


**Fig. S19** $^{1}$H NMR (400 MHz) spectrum of compound 2 in THF-$d_8$.

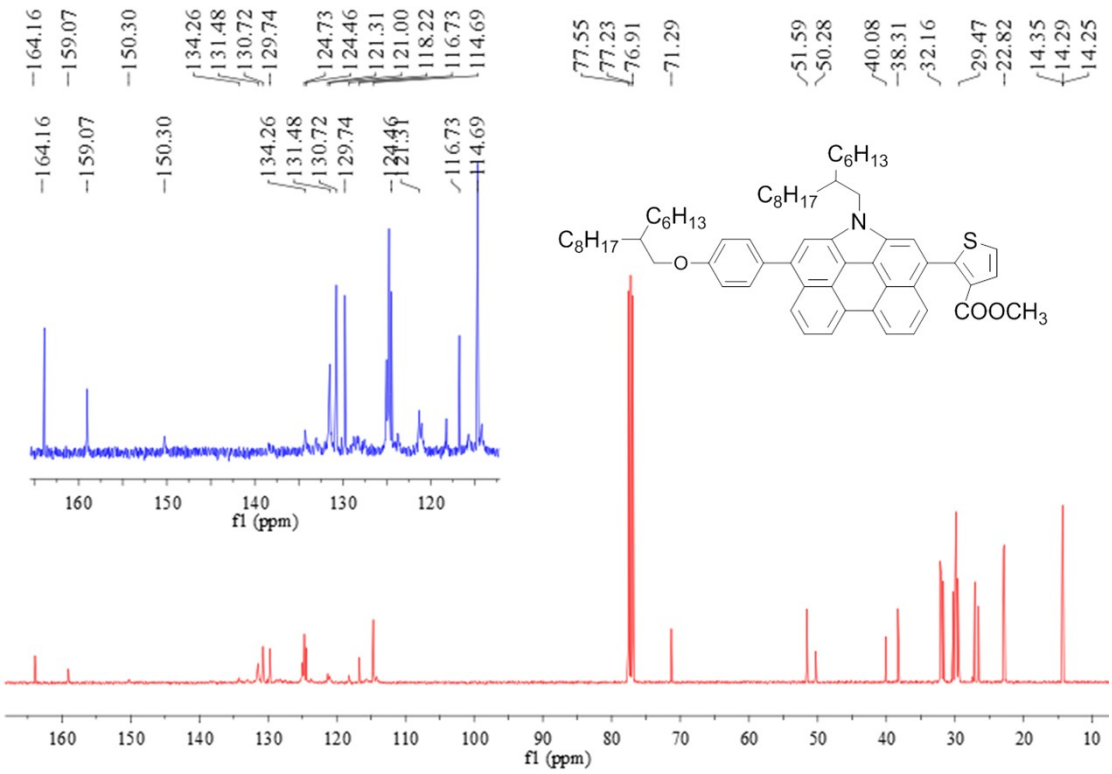


**Fig. S20** $^{13}$C NMR (100 MHz) spectrum of compound 2 in THF-$d_8$.

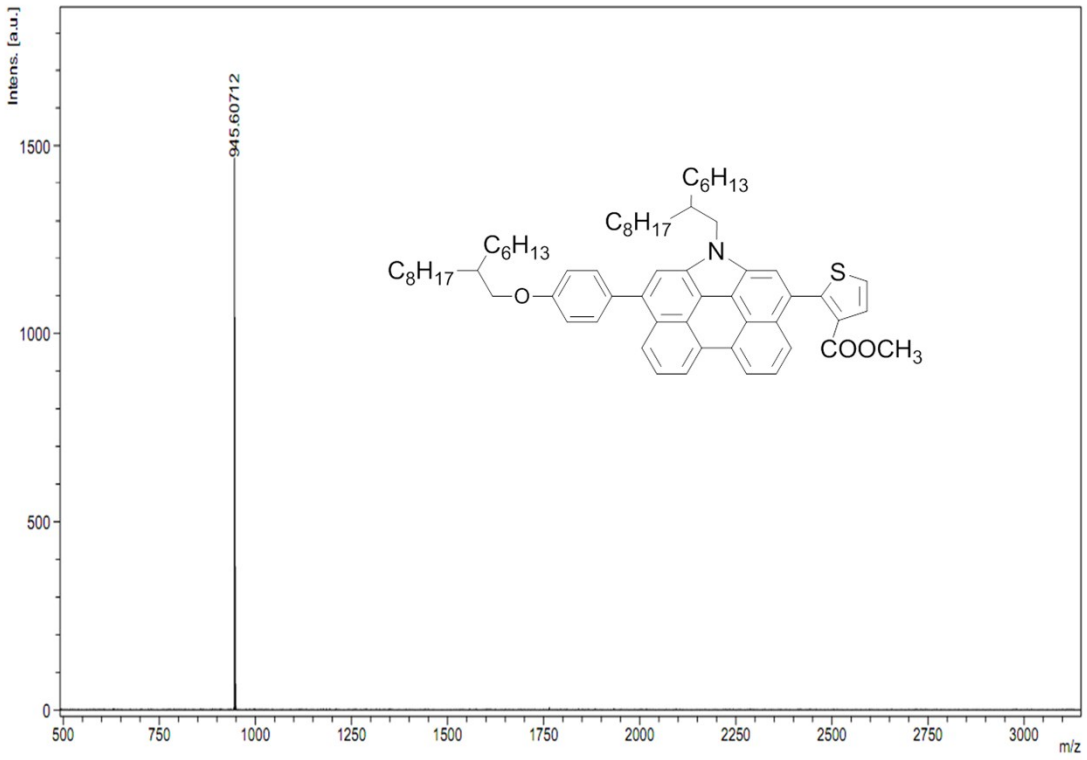


**Fig. S21** High resolution mass spectrum (MALDI-TOF) of compound 2.

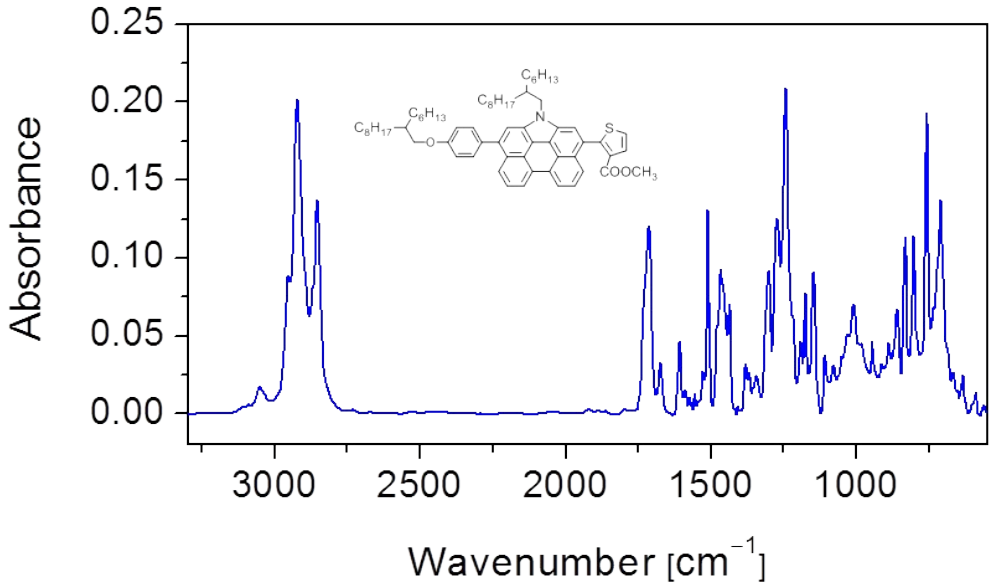


**Fig. S22** ATR-FTIR spectrum of compound 2.

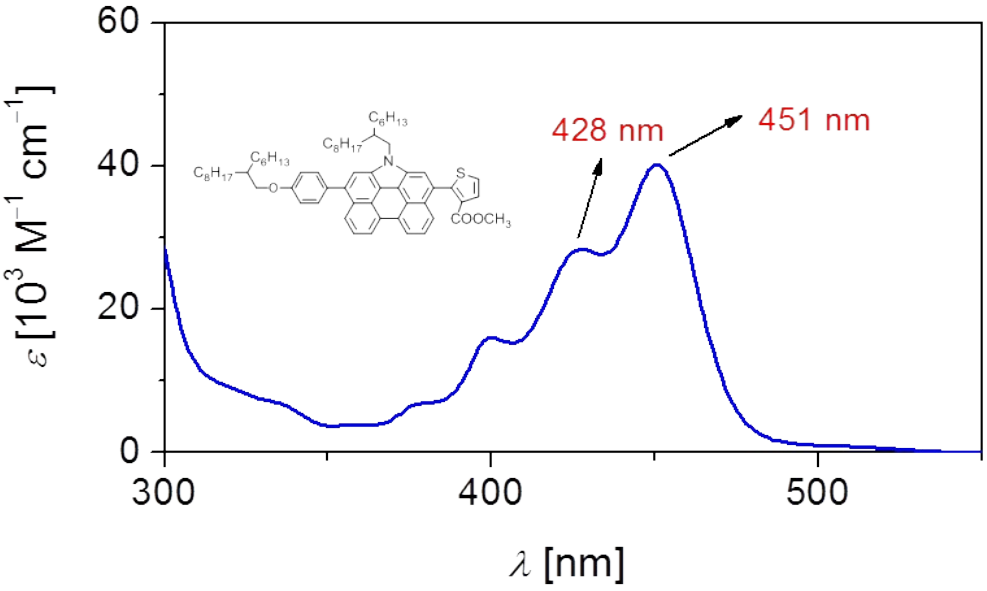


**Fig. S23** UV-Vis absorption spectrum of compound 2 (10 μM) in THF.

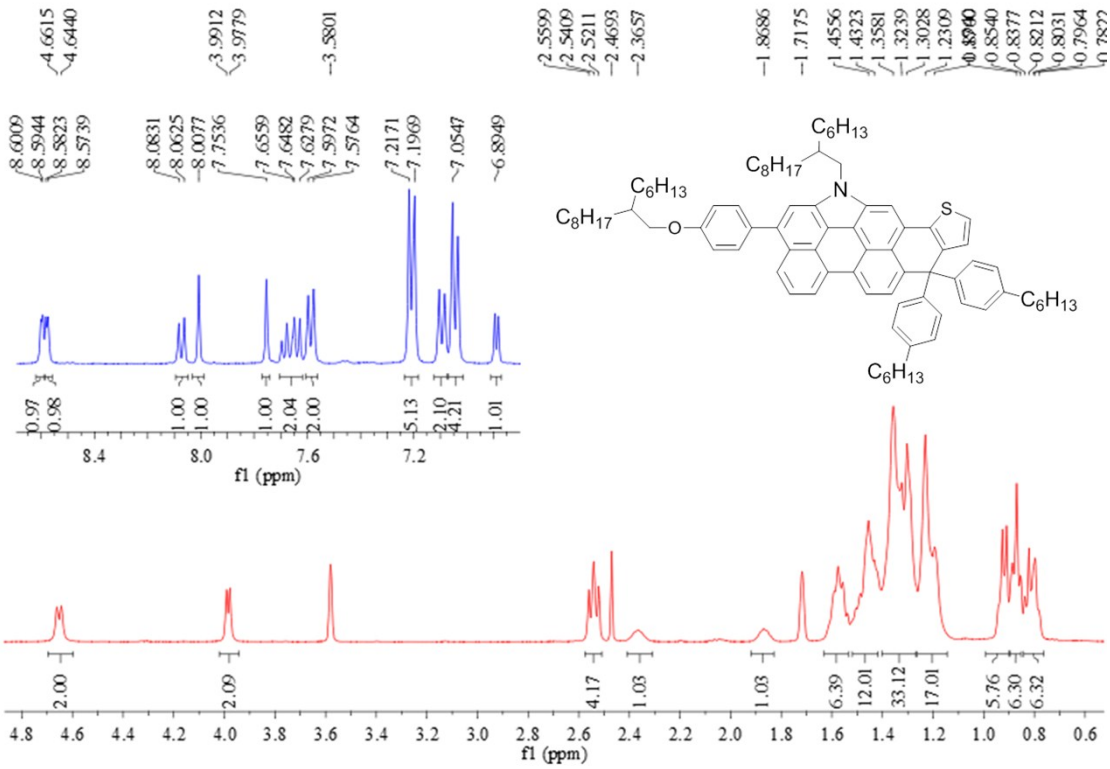


**Fig. S24** $^{1}$H NMR (400 MHz) spectrum of compound 3 in THF-$d_8$.

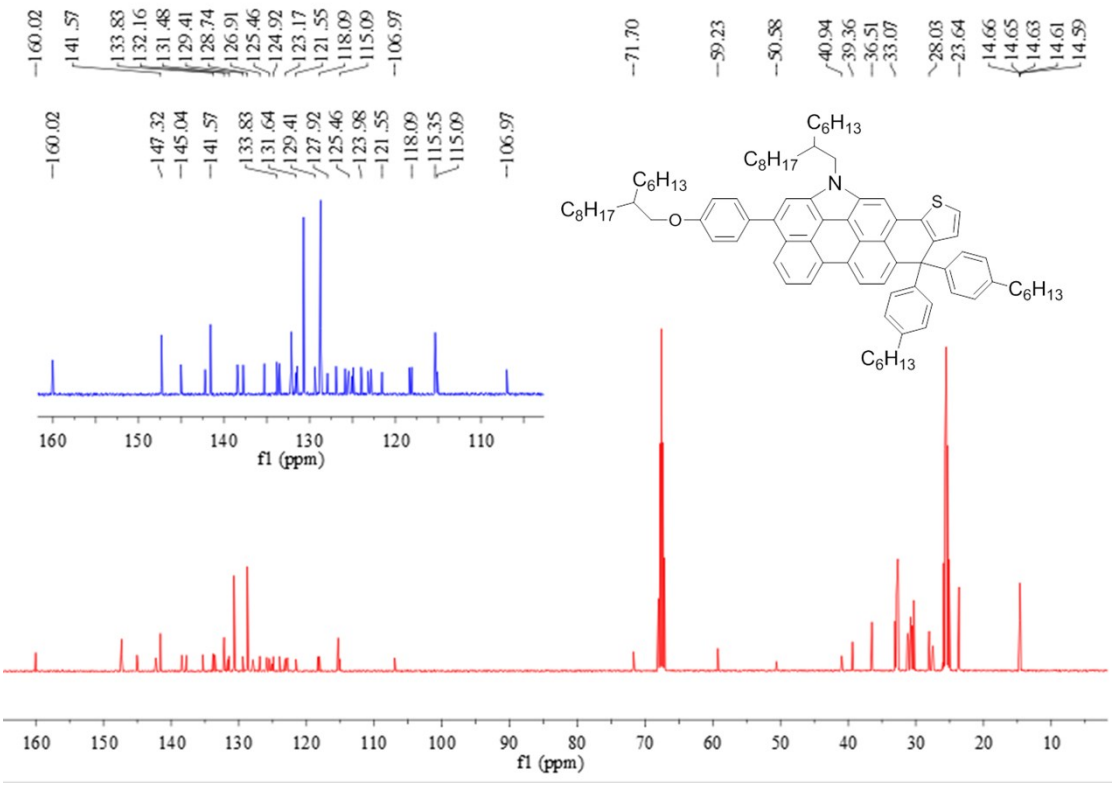


**Fig. S25** $^{13}$C NMR (100 MHz) spectrum of compound 3 in THF-$d_8$.

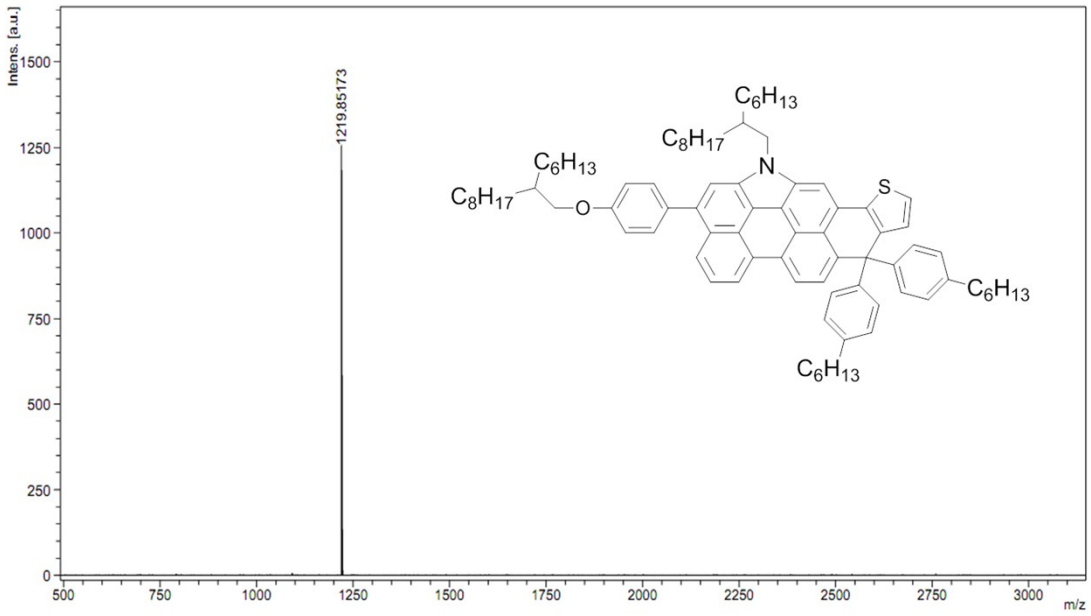


**Fig. S26** High resolution mass spectrum (MALDI-TOF) of compound 3.

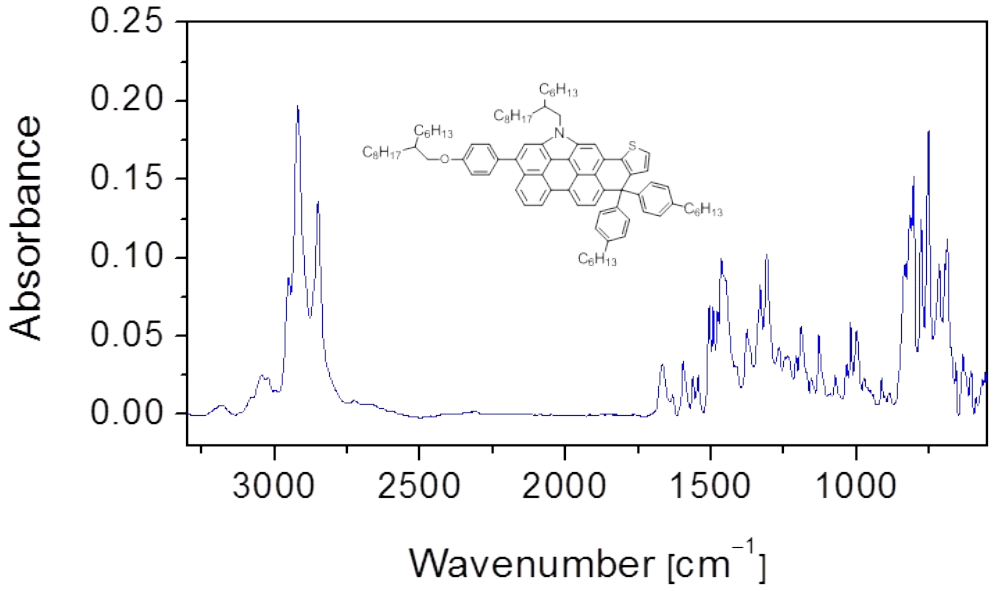


**Fig. S27** ATR-FTIR spectrum of compound 3.

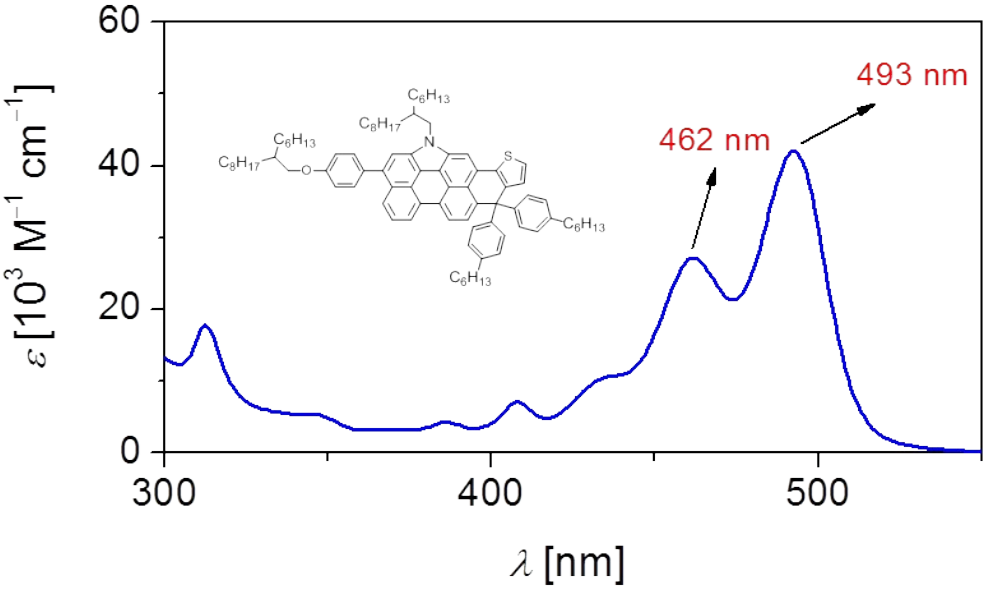


**Fig. S28** UV-Vis absorption spectrum of compound 3 (10 μM) in THF.

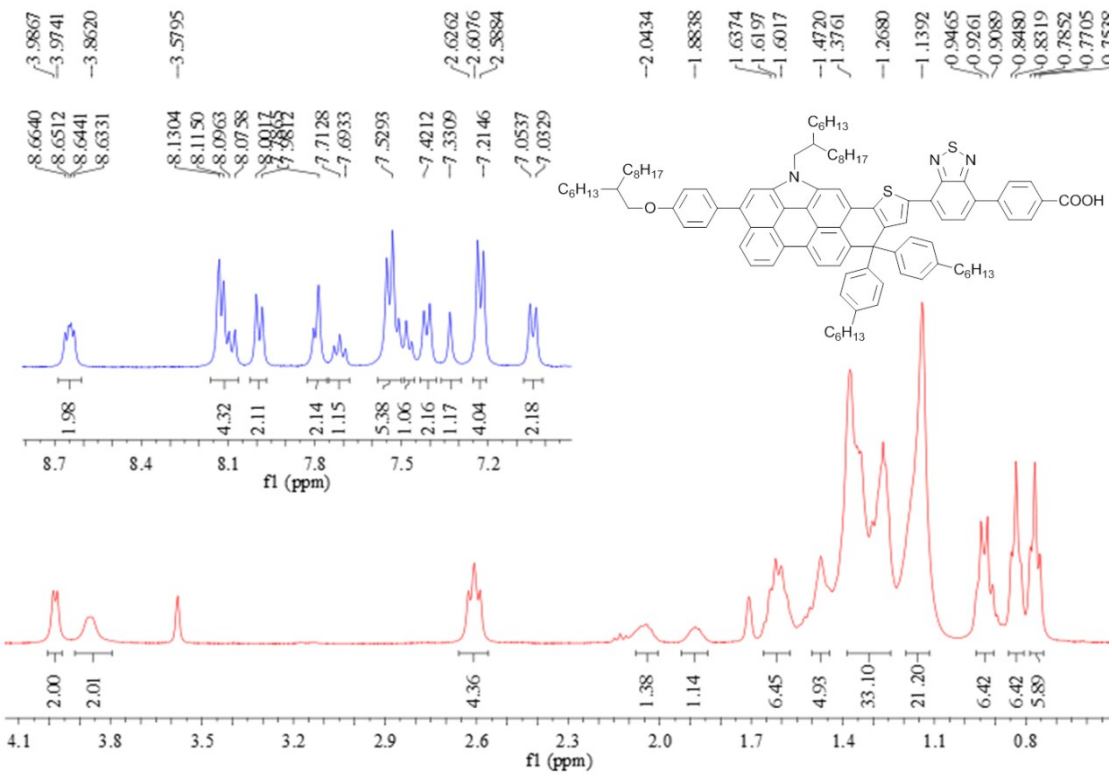


**Fig. S29** $^{1}$H NMR (400 MHz) spectrum of C296 in THF-$d_8$.

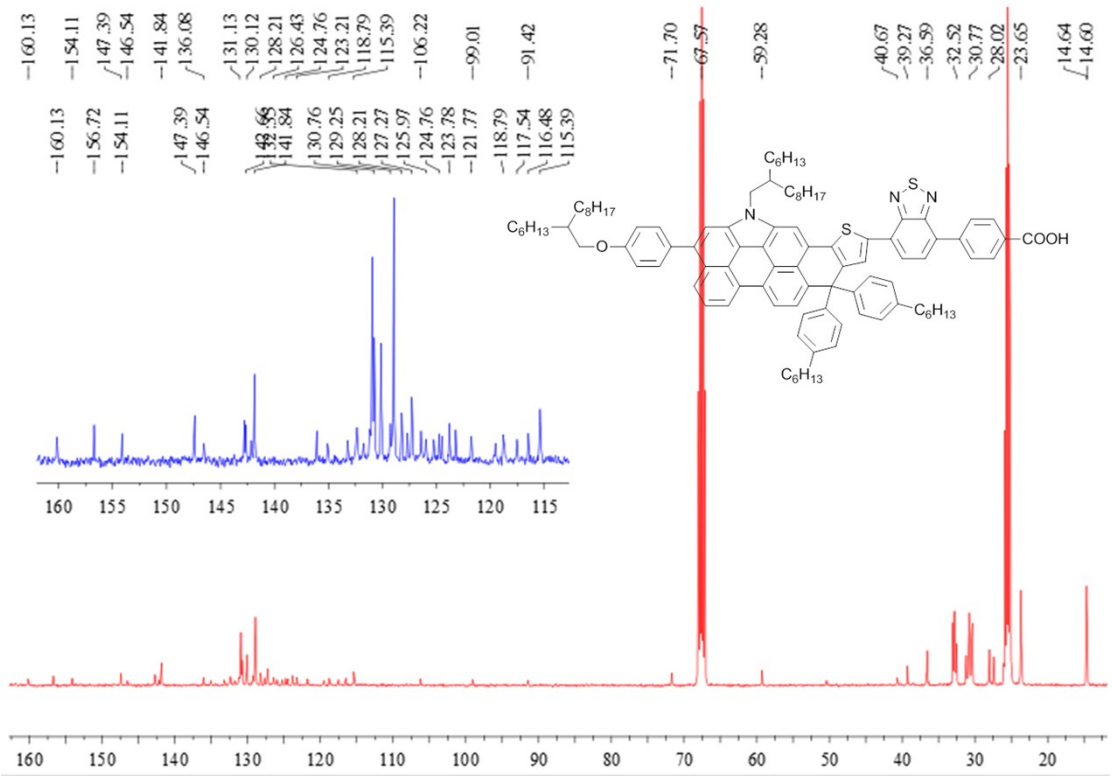


**Fig. S30** $^{13}$C NMR (100 MHz) spectrum of C296 in THF-$d_8$.

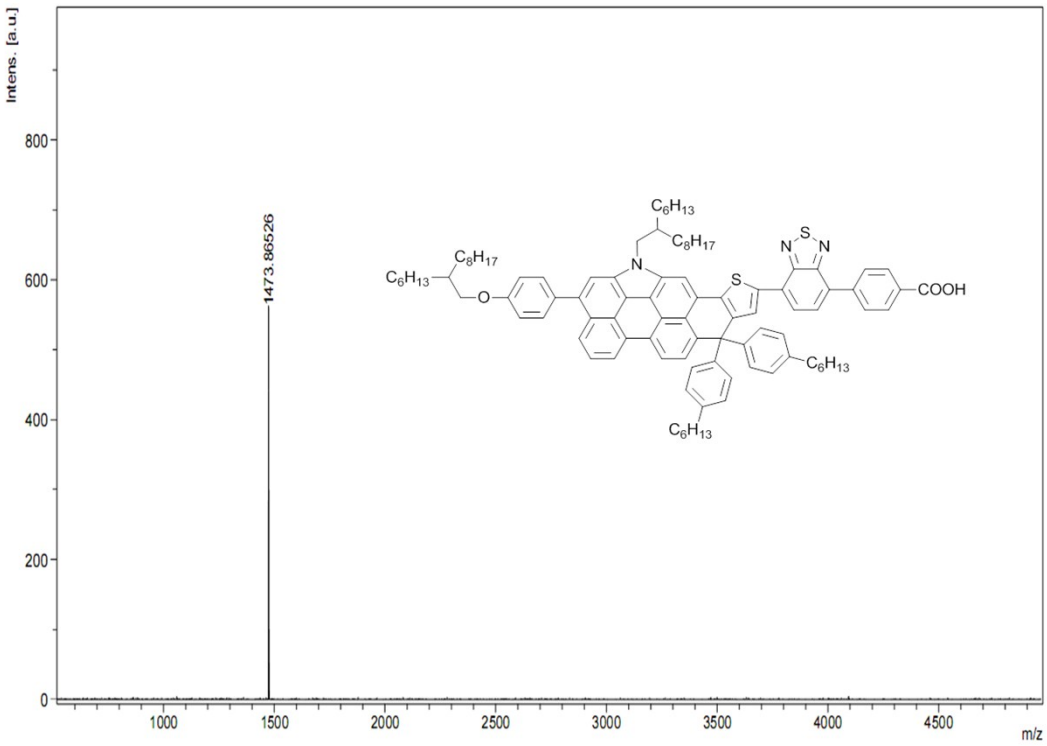


**Fig. S31** High resolution mass spectrum (MALDI-TOF) of C296.

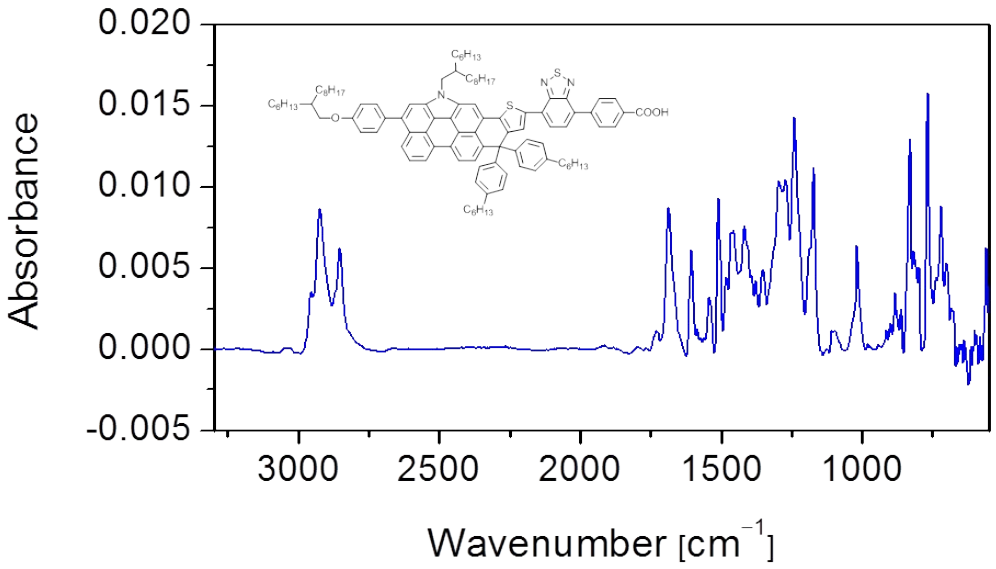


**Fig. S32** ATR-FTIR spectrum of C296.

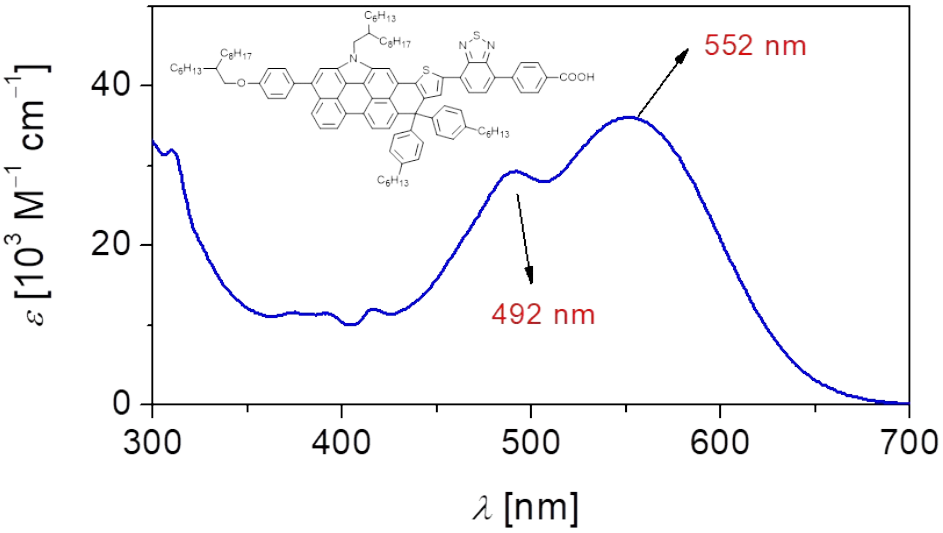


**Fig. S33** UV-Vis absorption spectrum of C296 (10 μM) in THF.

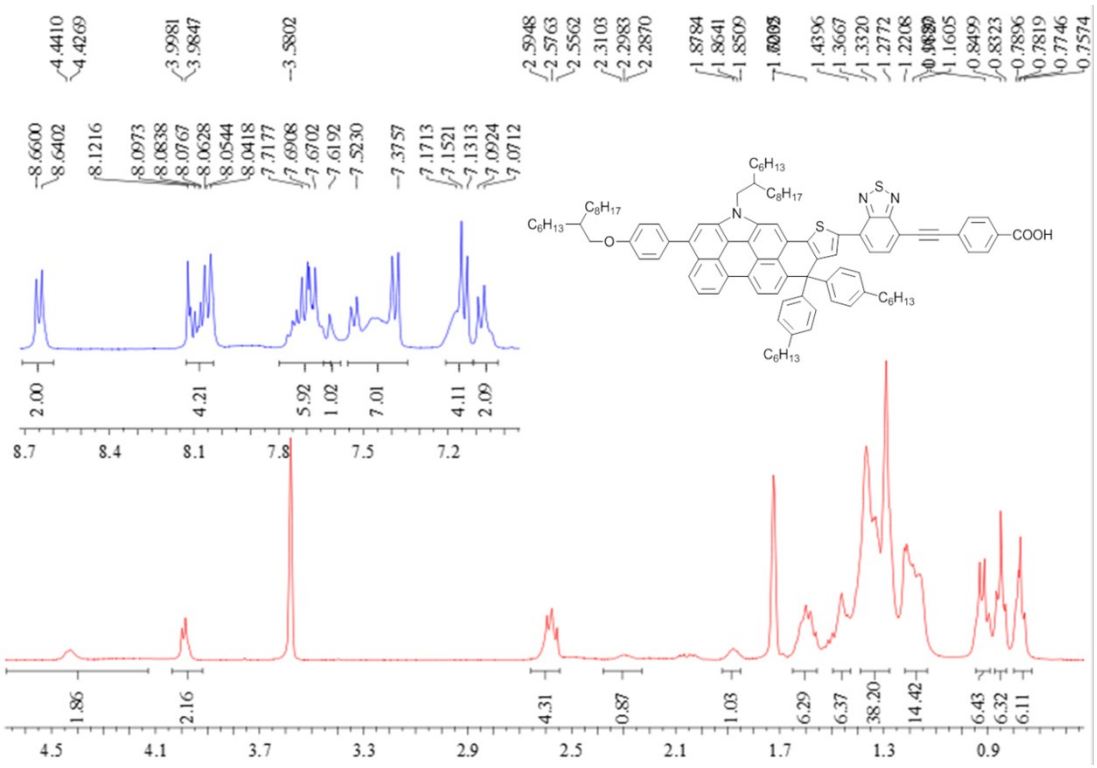


**Fig. S34** $^{1}$H NMR (400 MHz) spectrum of C298 in THF-$d_8$.

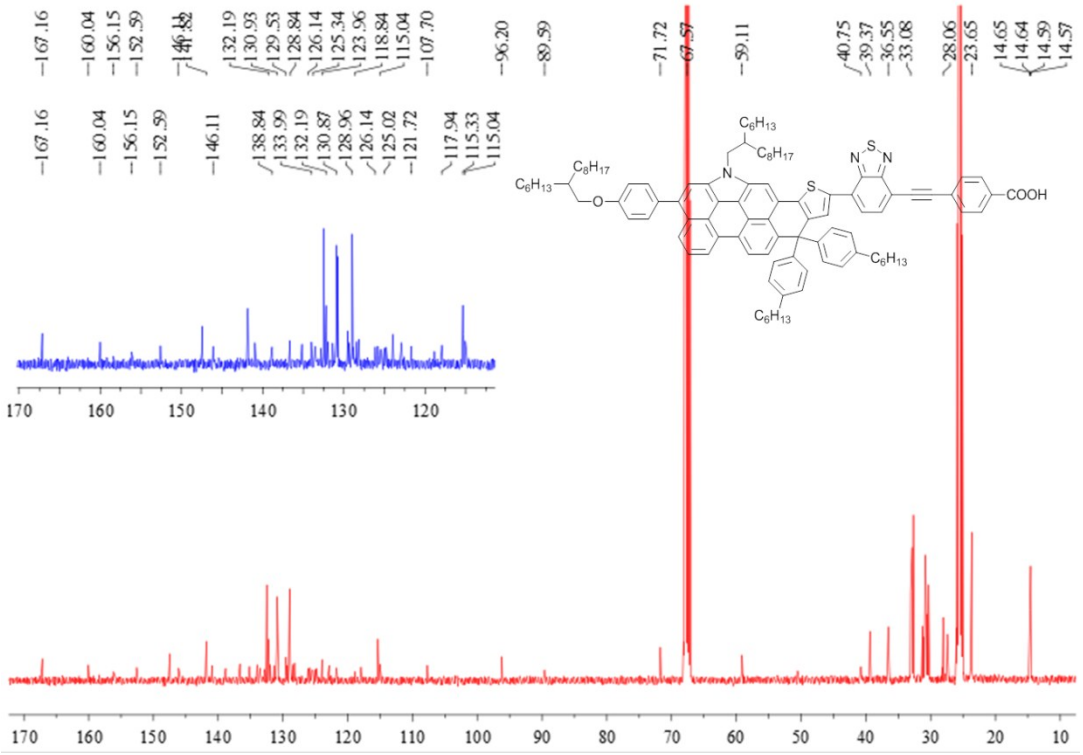


**Fig. S35** $^{13}$C NMR (100 MHz) spectrum of C298 in THF-$d_8$.

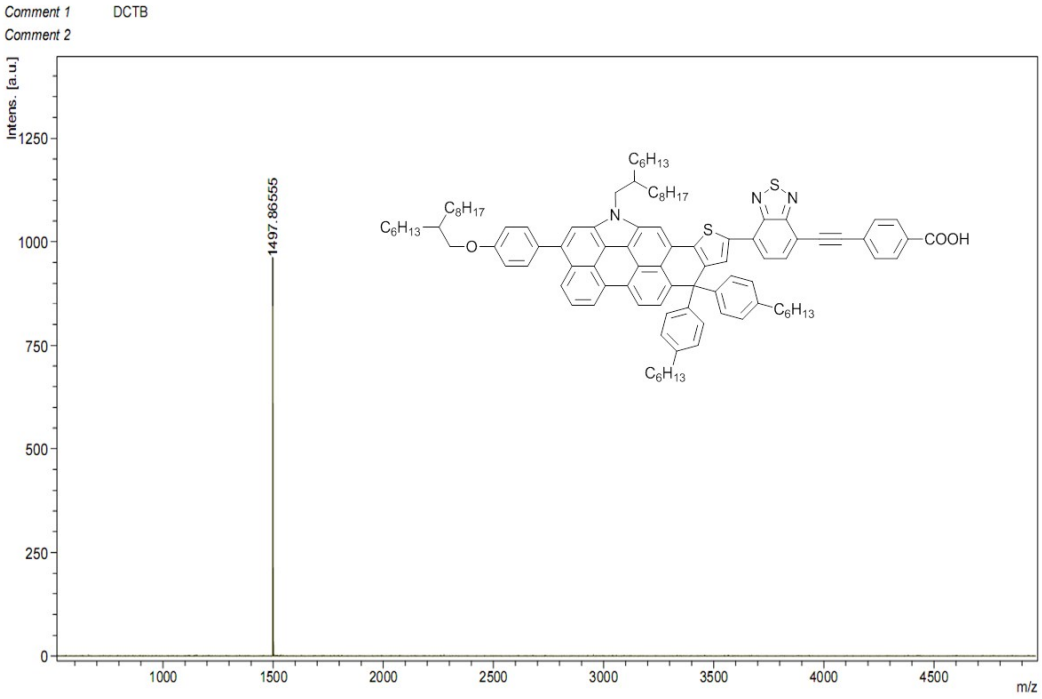


**Fig. S36** High resolution mass spectrum (MALDI-TOF) of C298.

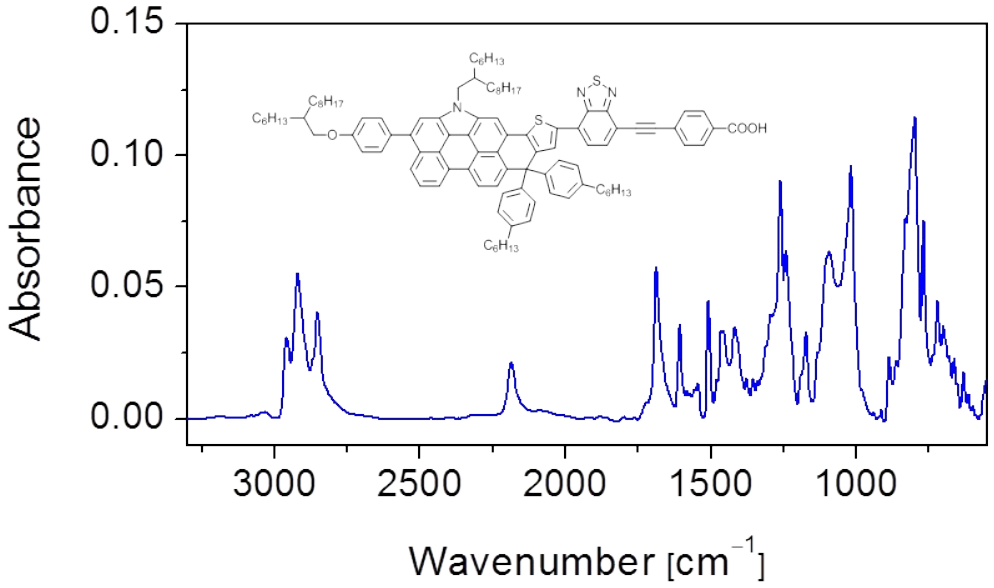


**Fig. S37** ATR-FTIR spectrum of C298.

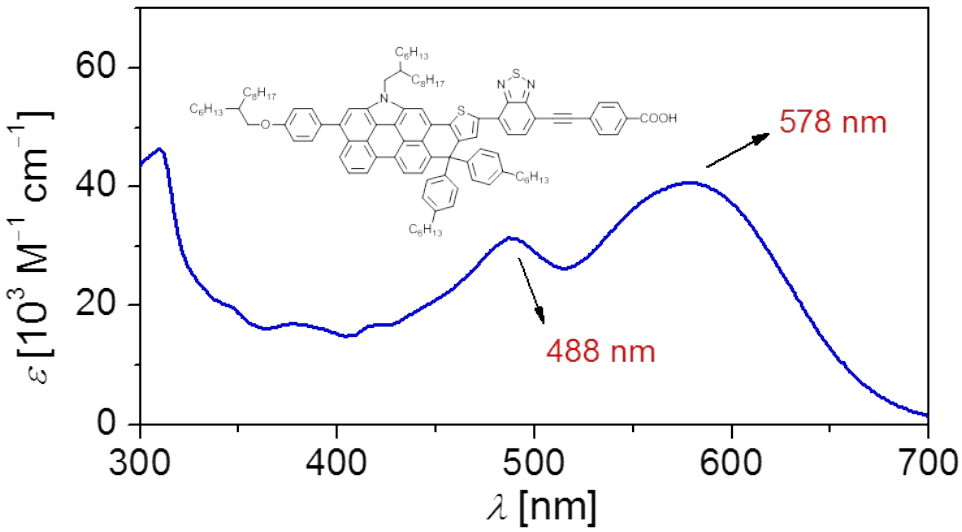


**Fig. S38** UV-Vis absorption spectrum of C298 (10 μM) in THF.